Microbial and Metabolic Succession on Common Building Materials Under High Humidity Conditions

Simon Lax[1*#], Cesar Cardona[2,3#], Dan Zhao[4], Valerie J. Winton[5], Gabriel Goodney[6], Peng Gao[5], Neil Gottel[3], Erica M. Hartmann[7], Chris Henry[8], Paul M. Thomas[5], Scott T. Kelley[6], Brent Stephens[4$], Jack A. Gilbert[3$]

[1] Department of Ecology and Evolution, The University of Chicago
[2] Graduate Program in Biophysical Sciences, The University of Chicago
[3] Department of Surgery, The University of Chicago
[4] Department of Civil, Architectural and Environmental Engineering, Illinois Institute of Technology
[5] Proteomics Center of Excellence and Department of Molecular Biosciences, Northwestern University
[6] Department of Biology, San Diego State University
[7] Department of Civil and Environmental Engineering, Northwestern University
[8] Mathematics and Computer Science, Argonne National Laboratory
[*] Present Address: Center for the Physics of Living Systems, Department of Physics, MIT
# These authors contributed equally to this work
[$] Co-corresponding Authors: brent@iit.edu; gilbertjack@gmail.com.

ABSTRACT

Despite considerable efforts to characterize the ecology of bacteria and fungi in the built environment (BE), the metabolic mechanisms underpinning their colonization and successional dynamics remain unclear. Here, we applied bacterial/viral particle counting, qPCR, 16S and ITS rRNA amplicon sequencing, and metabolomics to longitudinally characterize the ecological dynamics of four commonly used building materials maintained at high humidity conditions (~94% RH). We varied the natural inoculum provided to each material by placing them in different occupied spaces, and we wet the surface of half of the samples of each material to simulate a flooding event. As expected, different materials showed different bacterial and viral particle abundance, with wet materials having higher growth rates and lower alpha diversity compared to non-wetted materials. Wetting described the majority of the variance in bacterial, fungal and metabolite structure, and material type only influenced bacterial and metabolic diversity, while location of inoculation was only weakly associated with bacterial and fungal beta diversity. Metabolites indicative of microbial activity were identified, as were those that were native to the surface material. Glucose-phosphate was abundant on all materials (except mold-free gypsum) and was correlated with *Enterobacteriaceae*, which could indicate a potential bacterial nutrient source. A compound consistent with scopoletin, a plant metabolite with antimicrobial activity, was significantly negatively correlated with *Bacillus* and positively correlated with *Pseudomonas* and enriched in medium density fiberboard (MDF) materials. In wet samples, the alkaloids nigragillin and fumigaclavine C, both with antimicrobial properties, were significantly positively correlated with the fungal phylum Ascomycota. Nigragillin, was also negatively correlated with *Bacillus* and *Pseudomonas* abundance. Thiabendazole and azoxystrobin (anti-fungal compounds) were highly abundant on mold-resistant gypsum wallboard and likely directly influenced the decreased fungal growth observed on this material. The mold-resistant gypsum material also showed a significant increase in bacterial alpha diversity, and bacterial and viral particle abundance, as well as a decrease in metabolite diversity, likely a result of reduced fungal growth. *Penicillium* taxa were positively correlated with thiabendazole, which suggested the persistence of resistant strains. Also,

specific to the wet samples, *Bacillus* abundance was positively correlated with the azoxystrobin, suggesting bi-directional competitive adaptation, and positively correlated with metabolites known to interfere with *Pseudomonas* biofilm formation, which could explain the anti-correlation between these taxa. As expected, high moisture conditions enabled faster growth of inoculating microorganisms, whose composition, chemistry, and competition was shaped by surface material, suggesting that both fungal and bacterial growth need to be considered when determining the impact of dampness in built environments.

INTRODUCTION

The microbiology of the built environment comprises bacteria, archaea, fungi, viruses and protists, all of which maintain growth potentials under varying physicochemical regimes. Many recent studies of this ecosystem have applied molecular sequencing techniques to characterize microbial community relationships and dynamics under varying occupant density, building type and location, environmental conditions, and material type (Lax *et al.*, 2017; Adams *et al.*, 2016; Chase *et al.*, 2016; Stephens, 2016; Lax *et al.*, 2014). However, most of these studies have investigated communities sampled from relatively dry materials on which microbes are likely biologically inactive unless they experience liquid water or high relative humidity (RH) (Chase *et al.*, 2016). It is widely accepted that fungal growth can occur at RH >75-80% and material decay can occur at RH >95%, depending on material (Viitanen *et al*., 2010, Johansson *et al.*, 2012).

Dampness is a fairly common occurrence in buildings, with approximately half of all homes in the U.S. having experienced dampness or mold (IAQ Report - Prevalence of Building Dampness). Building material dampness occurs for different reasons, including: bulk liquid entry from floods, extreme weather events, and plumbing system problems; rain or snow entry through leaks in building envelopes and roofing systems; and high water vapor content resulting from moisture migration through building materials or condensation of warm humid air on cold surfaces (IAQ Report - Nature and Causes of Building Dampness). Dampness and the presence of visible mold have been consistently associated with adverse human health outcomes, including respiratory and allergic effects (Mendell *et al.,* 2011, Quansah *et al.*, 2012, Fisk *et al.*, 2010, Jaakkola *et al.*, 2013). Hypotheses to potentially explain these associations include a combination of exposure to specific microbial agents (Institute of Medicine, 2004), varied gene expression and metabolism (Hegarty *et al.*, 2018), and the release of fungal metabolites including mycotoxins (Miller *et al.*, 2014) and microbial volatile organic compounds (mVOCs) (Roze *et al.*, 2013).

Although fungal growth on building materials has been studied for decades (Hyvärinen *et al.*, 2002, Gravesen *et al.*, 1999, Hoang *et al.*, 2010; Pasanen *et al.*, 1992), only a limited number of studies have used molecular techniques to investigate bacterial and fungal growth, microbial community dynamics, and/or metabolic activity on common buildings materials exposed to liquid water and/or high humidity conditions (Coombs *et al.*, 2017). Therefore, we characterized the bacterial and fungal concentration and diversity, as well as the production of microbial metabolites, on samples of four common building materials incubated at ~94% relative humidity: oriented strand board (OSB), medium density fiberboard (MDF), gypsum wallboard, and mold-resistant gypsum wallboard. We varied the BE source of inoculation and purposely wet half of the samples to assess how indoor microbial sources and the presence of liquid water influence community structure and metabolite profiles of these materials over multiple time points. We used several techniques to quantify microbial growth and microbial community composition and functional metabolism including: bacterial and viral like particle counts, image processing of visible mold

74 growth, qPCR, amplicon sequencing of 16S and ITS rRNA marker genes, and metabolomics.
75 Results from these different methods were integrated via co-occurrence network approaches,
76 which provided insights into microbial community organization and environmental interaction.
77 Improved understanding of how bacterial and fungal metabolism is shaped by environmental
78 properties (e.g., the presence of water, surface material composition) and inoculating source (e.g.,
79 building location, occupancy patterns) could have important implications for architectural design,
80 construction, building management, and occupant health (Rand *et al.*, 2017). Therefore,
81 determining the microbial metabolic dynamics in these high RH environments should be an
82 important research priority.
83

84 **RESULTS**
85

86 *Experimental Setup*
87

88 Our study used four building materials types: oriented strand board (OSB), medium density
89 fiberboard (MDF), regular gypsum wallboard, and mold-resistant (i.e., mold-free, or 'MF')
90 gypsum wallboard. Coupons of 5 cm × 5 cm of each material type were naturally inoculated at
91 two different locations for about 50 days each. After the inoculation period concluded, the time
92 that occupants were coming in close proximity was reported with similar values, a 0.16% and
93 0.18% of total time. The material coupons were sampled for off-line biological and chemical
94 analysis at 7 different sampling time points, referred to here as TP0, TP1, TP2, TP3, TP4, TP5,
95 and TP6. The initial samples (TP0) were taken just after retrieving the samples from the field
96 inoculation and represent non-wetted, naturally inoculated samples previously held at normal
97 residential humidity condition. After inoculation, half of each set of materials from each location
98 were submerged in tap water in separate pans for ~12 hours to simulate the process of wetting of
99 building materials due to a flood or leak. Different sampling strategies were tested and after
100 statistical verification all samples of the same type were combined as technical replicates (**Figure**
101 **S1**). Microbial datasets were later rarefied to same sequencing depth: 1,000 reads for bacteria and
102 10,000 reads for fungi. Unfortunately, rarefaction removed all bacterial samples from MDF
103 materials, which had very low read counts. After rarefying the data, a comparison of the control
104 and non-control samples reflected that control samples looked very similar in bacterial and fungi
105 diversity than non-control samples, (mantel >= 0.49 and >= 0.43 for location 1 and location 2
106 respectively, all with a $p < 1E-05$), perhaps because air could still transmit through the non-
107 hermetic foil cover and microbes from the interior of the wood (not killed with the sterilization)
108 could have found their way to the surface. Highlighting that the coupon itself could still be an
109 important contributor to microbial diversity for all samples. From these results, the control location
110 was treated indistinctly than the other two locations. For more details see Materials and Methods
111 section.
112

113 *Visible growth, particulate counts and qPCR*
114

115 Visible microbial growth occurred much faster and covered a far greater percentage of the surface
116 area on wet tiles than on non-wetted tiles (**Figure 1A**). OSB and MDF had the greatest coverage
117 and fastest growth: all wet OSB and MDF tiles reached at least 50% visible microbial coverage by
118 day 20, while non-wetted tiles of these types reached < 25% coverage. No growth was ever visible
119 on the mold-resistant gypsum tiles. Epifluorescence microscopy revealed that counts of bacterial

like particles (BLP) and viral-like particles (VLPs) calculated on samples TP0 to TP3 were strongly correlated ($R^2 = 0.65$, $p = 2.8e^{-23}$) (**Figure 1B**), with VLP counts statistically lower than bacterial counts in all samples (ANOVA $<=10^{-4}$) and in both wet and non-wet conditions (two sided non-parametric t-test $p <= 0.035$) **Figure 1C**). This is in keeping with previous research that found very low VLP:bacteria ratios in the indoor environment (Prussin *et al.*, 2015, Gibbons *et al.*, 2015). In our dataset, the mean VLP-bacteria ratio was 0.86 ± 0.07, with a minimum of 0.61 and a maximum of 1.02 across all samples.

While BLP (only estimated for TP0 to TP3 samples) and bacterial qPCR agree that wetted samples had higher counts than non-wetted samples, cell counts inferred from these two methods drastically differ for different material types and over time. Most notably, the MF-gypsum had the greatest BLP counts but also the lowest 16S rRNA qPCR counts (6-fold or more lower than other materials). Moreover, the BLP cell counts were essentially constant over time, while qPCR counts steadily increased, with TP6 being 4-fold greater than TP1 and 209-fold greater than TP0 counts. To further confirm the differences, we calculated the overall correlation between paired bacterial qPCR and BLP counts and the results were not significant, emphasizing different biases for each method.

For fungal qPCR we observed MF-gypsum had the lowest abundance, while all other materials had a range of 20 to 118-fold increase over MF-gypsum. Wetted samples revealed a 4-fold increase in qPCR read abundance over non-wetted samples. Also, the qPCR read abundance increased steadily over time, in such a way that TP6 was 11-fold greater than TP1 and 750-fold greater than TP0 counts.

Bacterial, fungal and metabolite diversity

The bacterial and fungal communities in our study tended to decrease in diversity over time, as measured by the Shannon Index (Shannon H'), which incorporates both the richness and evenness of the community. Given that our data was rarified to an even depth before analysis, this decrease in diversity is indicative of the increasing relative abundance of certain community members, and suggests the preferential proliferation of certain taxa in the inoculating community. In our 16S dataset, wet samples experienced faster declines in diversity than non-wetted samples, and were significantly lower in diversity at the end of the study than non-wetted samples (**Figure 2A**), suggesting that certain bacterial taxa grew quickly in the wet environment and became dominant within the community. In our ITS dataset, we also observed a faster decline in diversity in wet samples, although wet samples were significantly more diverse than non-wetted samples by the end of the study (**Figure 2B**). The decrease in fungal diversity in wetted samples was not monotonic, with an initially steep decline and a subsequent increase. This may reflect fast growth by a small number of taxa that quickly dominated the community, followed by the growth of other taxa with slower growth rates. Similar patterns are observed when looking at the diversity changes for each individual material (**Figure S2**) with the exception of a lack of bacterial growth for wet MDF samples and reduced bacterial growth on dry OSB after the study was half way completed. In contrast, we observed no significant changes in the metabolic diversity over time for either wet or non-wetted samples (**Figure 2C**).

Microbial Compositional Changes

Across all samples, the diversity of bacteria within the community was significantly correlated to the diversity of fungi (Corr = 0.28, p=0.0003) (**Figure 3A**). Interestingly, neither bacterial nor fungal diversity was significantly correlated to the metabolite diversity, perhaps because of a narrower range of observed metabolite diversity compared to the taxonomic datasets. We observed striking changes in the relative abundance of certain bacterial (**Figure 3B**) and fungal (**Figure 3C**) genera over time, which were largely dependent on wetting condition. In the 16S rRNA dataset, *Bacillus* almost immediately came to dominate wet samples, with an average relative abundance as high as 50% after the 2nd time point, even though it represented a negligible part of the community at the start of sampling. *Bacillus* abundance also increased in non-wetted samples, although to a much smaller extent. A similar pattern was observed for the genera *Pseudomonas* and *Erwinia*, which also represented a very small fraction of community diversity at the start of sampling but quickly increased in abundance in wet (but not non-wetted) samples. Interestingly, a very large percentage of reads from early time point samples, both wet and non-wet, were of chloroplast origin. In wet samples, the number of chloroplast reads quickly declined as the bacterial genera proliferated. In non-wetted samples, chloroplast read abundance remained high, and dominated the sequencing effort to such an extent that discarding those reads would have dropped the majority of non-wetted samples below the rarefaction depth. While these likely represent residual DNA signatures from the plant material used to construct each tile material, we have chosen to keep them in the analysis. **Figure S3A** shows how this dynamic slightly vary for each different material type.

The majority of reads in the ITS dataset that could be taxonomically assigned to a genus belonged to one of two genera: *Eurotium* and *Penicillium*. *Eurotium* abundance was negligible at the beginning of community succession but quickly flourished in non-wetted samples, becoming the most abundant known genus in those samples by time point 2 (**Figure 3C**). By contrast, *Eurotium* did not become abundant across wet samples. *Penicillium* abundance was, on average, consistently higher in wet samples than in non-wetted samples, and its abundance was significantly anti-correlated to *Eurotium* relative abundance (corr = -0.12, p = 0.033). These taxa-specific changes were mirrored by community level differentiation, where wet vs. non-wetted tiles of the same material and inoculating location became significantly more dissimilar (Bray Curtis, Spearman's Correlation, $p<0.01$) in both their bacterial and fungal community structure over time (**Figure 3D**). **Figure S3B** shows how this dynamic slightly vary for each different material type.

Environmental Factors Associate with Microbial and Metabolite Diversity

We used ANOSIM to calculate the factors significantly correlated with differences in the microbial communities across our three datasets. Bray-Curtis dissimilarity was calculated for the 16S, ITS, and metabolite datasets, and ANOSIM was used to determine whether distances between samples of the same metadata factor (i.e. wetting condition, inoculating location, and material) were significantly lower than distances between samples of different types (**Figure S4**). In our 16S rRNA dataset, wetting condition, location, and material each had a significant impact on bacterial community structure (all p <0.0001 based on 10^5 randomized permutations), with wetting having the most pronounced effect (R = 0.418). In general, non-wetted samples tended to be more similar to each other than wet samples were to each other, which is likely due to the dominance of a single

chloroplast OTU. Material had a less pronounced effect (R=0.247) and location had the least evident effect on bacterial community structure (R=0.133).

Interestingly, fungal community structure was not significantly described by variance in material, while location had a relatively weak (R = 0.129) though highly significant ($p < 0.0001$) association, suggesting that variations in fungal communities that settle on materials (which have been shown to be driven largely by outdoor fungal communities, e.g., Adams *et al.*, 2013) influence community structure upon experiencing wetting and high RH conditions. Wetting condition was by far the most influential factor influencing fungal community structure ($R = 0.564$, $p < 0.0001$), and in contrast to the bacterial data, wet samples were much more similar to each other than were non-wetted samples. Metabolite diversity within the community was also affected by wetting condition ($R = 0.276$, $p < 0.0001$), with non-wetted samples more similar to each other than wet samples. Material also played a significant role in metabolite diversity ($R = 0.231$, $p < 0.0001$), and mold-free gypsum samples were particularly metabolically similar, likely due to the lack of fungal growth and the underlying chemical composition of the material. Inoculating location had no significant effect on the diversity of metabolites despite having a significant effect on both the bacterial and fungal community membership. We visualized sample similarity using non-metric multi-dimensional scaling (NMDS) ordination based on Bray-Curtis dissimilarity (**Figure 4**). We converted material, location, and wetting condition into binary variables (1 = yes, 0 = no), which were fit onto the ordination, keeping only the significant vectors (R^2 values for each vector and their significance is presented in **Table S1)**. Visually, both bacterial and fungal beta diversity was more differentiated by wetting condition due to the significant increase in growth on wetted tiles, while metabolites were visually differentiated by both wetting condition and surface material, likely due to the underlying chemistry of the material and then the subsequent metabolic activity of the microbes when tiles were wetted.

Bacterial and fungal network co-occurrence

Using SparCC (Friedman & Alm, 2012), an algorithm developed to quantify correlations on microbial compositional data (data that has been subject to rarefaction), and a correlation threshold >0.4, uncovered co-occurrence patterns between taxa from each kingdom. In the bacterial network (**Figure S5**) three co-occurrence clusters were identified, the *Bacillus* cluster, *Pseudomonas* cluster, and a cluster comprising chloroplasts and mitochondria. As expected these groups correspond with the most abundant taxa. On all wet materials and on all samples of gypsum (both wet and non-wet), 95% of associations between *Bacillus* and *Pseudomonas* were negative correlations (**Figure S6 and S7**). On non-wetted OSB, MDF and MF-Gypsum there were no negative correlations between *Pseudomonas* and *Bacillus.* Interestingly, there is a dramatic increase in the absolute number of significant co-occurrence relationships between bacterial OTUs in wet (74) versus non-wetted samples (48), which is a 54% increase in the number of edges. In the fungal correlation network, *Penicillium* OTUs co-occurred with many unknown fungal genera, while OTUs corresponding to *Aspergillus* and its subset, *Eurotium,* maintained monophyletic clusters (**Figure S8**). As with the bacterial co-occurrence networks, fungal OTUs associated with wet tiles had negative correlations among each other, although the number was much smaller than for bacteria. Only 7 fungal OTUs were negatively correlated on wet materials, mainly between unknown genera and an abundant *Penicillium* OTU (**Figure S9**). Strikingly, unlike bacteria, the absolute number of significant co-occurrence relationships between fungal OTUs declined in wet

(555) versus non-wetted samples (1,133), which was a 104% decrease in the number of edges, suggesting an inverse co-abundance response between bacteria and fungi during growth.

To better understand the co-associations between bacteria and fungi, 16S and ITS OTUs were co-correlated in a single network. A random walk-based method uncovered four distinct modules within the network, with a modularity of 0.45 (**Figure 5A**). In general, the taxa present in each sample tended to cluster within an individual network module (median sample association to module = 0.88). We correlated various metadata factors to module membership (**Figure 5B**) and observed that wetting condition had a significant impact on which samples dominated each module: modules 1 and 3 were associated with wet samples, while modules 2 and 4 were associated with non-wetted samples (**Figure 5C**). Location 1 samples dominated module 3, while Location 2 samples dominated module 1 (**Figure 5D**). Overall, wetting condition appears to be the most important factor driving community succession, resulting in two different community structures even when the source community is identical. We also visualized the nodes that were assigned to the genera previously discussed in Figure 3. Nodes in the bacterial genera *Bacillus, Pseudomonas*, and *Erwinia*, as well as the fungal genus *Penicillium*, were nearly exclusively enriched in the two wet-associated modules (1 and 3), while chloroplast reads and *Eurotium* nodes all clustered within the non-wetted modules (2 and 4; **Figure 5E)**.

Metabolite network co-occurrence

A co-occurrence network correlation was calculated for the sample metabolite profiles (**Figure 6)**. As these data are not compositional, we built this network using significantly positive Spearman correlations between nodes and included only the 1,000 most abundant metabolites in the dataset. This resulted in a network with 149,316 edges (density = 0.30) when the significance threshold (alpha) was set to 0.001. Using the same module discovery method described above, we uncovered 7 distinct modules (modularity = 0.32), excluding 12 metabolites around the periphery of the network that clustered into modules of <5 nodes. Three modules (3, 4, and 7) were significantly correlated with wet samples, while modules 1, 2, 5 and 6 were associated with non-wetted samples. There was almost no correlation between network modules and inoculating locations, further suggesting that while location (and hence the primary inoculating microbes) may influence community taxonomic diversity, it does not appear to strongly affect metabolic diversity during growth. The abundance of metabolites in module 7 were anti-correlated with all other modules, but specifically with module 2 (corr =-0.87, p<0.001). Module 7 is dominated by wet samples at later time points, suggesting that community succession in wet environments may converge to a common metabolic profile, which is wholly distinct from the non-wetted samples in module 2.

Metabolite features can predict sample type

Random Forest analysis was employed to determine the metabolites associated with various sample types. Models classifying whether a sample was wet had an average accuracy of 98% (error ratio = 25, with expected random error 0.5), and wet-samples were never misclassified as a non-wetted sample in any of the 10 model iterations. Models classifying samples based on material were similarly successful, with an average accuracy of 97% (error ratio = 25, with expected random error 0.75). Metabolomics models were much less successful at predicting the inoculating location, with a mean success of 72% (error ratio = 2.36 with expected random error 0.67). We sought to gain insight into the chemical composition of metabolites that comprise the signatures

observed in these models. Feature importance scores were assigned to compounds based on their relative contributions to predicting sample type. For both the wetting condition dependent and material dependent groups, we selected the 100 highest-scoring metabolite features for further examination and chemical identification (**Figure S10**). Wet samples were enriched with 98 of the 100 top-scoring metabolites that differentiated wet and non-wetted. None of these compounds were automatically identified by mzCloud, so the metabolites were analyzed via external database searches, and compound classes were designated based on fragmentation spectra. A diverse set of compound families was observed, including compounds likely to be carbohydrates and glycoconjugates, fatty acids, prenol lipids, sterol lipids, polyketides, and glycerolipids, as well as several pyridine derivatives including a form of vitamin B6, indicative of microbial activity and growth and compounds associated with the surface materials.

Metabolites that were highly enriched in wet vs non-wetted conditions underwent additional manual analysis for confident structural identification. One of these metabolites was identified as Nigragillin ($C_{13}H_{22}N_2O$, accurate mass = 222.1723), which is a fungal alkaloid first identified in *Aspergillus niger* (Isogai *et al*., 1975). Nigragillin abundance was significantly enriched in wet MDF and OSB samples (505- and 280-fold, respectively) compared to non-wetted samples. However, no significant differences in nigragillin were observed for gypsum or MF-gypsum. In both wet MDF and OSB the nigragillin concentration increases over time **(Figure S11)**. Another high-scoring metabolite showed MS/MS fragmentation consistent with Fumigaclavine C ($C_{23}H_{30}N_2O_2$, accurate mass = 366.2291), which is a fungal alkaloid first identified in *Aspergillus fumigatus* (Cole *et al*., 1977). Fumigaclavine C was enriched in wet samples of gypsum, MDF, and OSB (23-, 26-, and 13-fold increase in comparison to non-wetted samples, respectively), with equivalent abundance in mold-free gypsum regardless of wetting. While the concentration of Fumigaclavine C remained flat or increased slowly in most materials, wet gypsum showed a dramatic increase in abundance at TP3 and 4 **(Figure S11).**

Metabolites that were predictive of material type (OSB, MDF, Gypsum and MF-Gypsum) were also further analyzed to determine how these materials influence the chemical composition of metabolites. Of these metabolites, 80% eluted with a retention time of >7 minutes, indicating a skew toward more hydrophobic compounds. This suggests that hydrophobic compounds are more diverse between the materials and therefore could have greater influence on microbial metabolism than the ubiquitous hydrophilic components. Two of these metabolites were identified by MzCloud search: glucose-phosphate, which was about 10-fold less abundant in MF-gypsum compared to all other materials, and scopoletin, a metabolite produced by the plants with antimicrobial activity Lerat *et al.*, 2009, Gnonlonfin *et al.*, 2012, Nascimento *et al.*, 2013), which was about 60-fold more abundant in MDF samples than in other materials and could be influencing the reduced bacterial growth on this material **(Figure S11)**. Thiabendazole and azoxystrobin, known anti-fungal compounds (Clausen & Yang, 2007, Balba, 2007), were highly overrepresented on MF-Gypsum, 333 and 595-fold respectively more abundant than the average content for the other three materials, and as such are likely some of the active compounds in MF-Gypsum.

Microbe-metabolite co-occurrences

The abundances of Nigragillin and Fumigaclavine C were each significantly positively correlated with a fungal OTU annotated to the phylum Ascomycota (corr = 0.66, FDR p = 0.0004), which

contains species known to produce such alkaloids. Both Nigragillin and Fumigaclavine C have been reported to display antibacterial activity (Magdy *et al.*, 2017 & Pinheiro *et al.*, 2013). Interestingly, Nigragillin was negatively correlated with the abundance of *Bacillus* and *Pseudomonas* OTUs; this could suggest fungal competition for space and resources (Mille-Lindblom *et al.*, 2006) against bacteria, and in the specific case of MDF, when Nigragillin abundance was greatest no bacterial growth was detected **(Figure S2, Figure S11).** The abundance of glucose-phosphate was significantly correlated to the proportion of a dominant Enterobacteriaceae OTU, a genus which is known to synthesize it (Herter *et al.*, 2006) (corr = 0.72, FDR p = 0.000002). Thiabendazole was positively correlated with *Penicillium* abundance (corr = 0.80, FDR $p < 10^{-9}$). As thiabendazole is prevalent and persistent in the natural environment, this correlation may indicate the presence of thiabendazole-resistant *Penicillium* strains colonizing the material from the built environment (Holmes & Eckert, 1999).

Co-occurrence networks were constructed between the bacterial OTUs and metabolites (SparCC correlation of >0.4; **Figure S12**) to explore further specific microbe-metabolite associations and possible mechanistic interactions. Significant correlations were observed between *Bacillus* OTUs and lipids including fatty acids and monoacylglycerophosphocholine compounds, which are likely to indicate cell wall and biofilm formation (Diomande *et al.*, 2015, Dubois-Brissonnet *et al.*, 2016). Interestingly, *Bacillus* OTUs were also positively correlated to other lipid classes including diols and flavonoids, which have all been observed to interfere with *Pseudomonas* biofilm formation (Kong *et al*., 2014; Jensen *et al*., 2014). In addition, the abundance of two fatty acids, one diol, and azoxystrobin, were positively correlated with *Bacillus* and negatively correlated with *Pseudomonas*. Conversely, scopoletin was positively correlated with *Pseudomonas* and negatively correlated with *Bacillus* **(Figure S13).** These additional antagonistic compound interactions between *Bacillus* and *Pseudomonas* could represent either competitive interactions between these organisms or different adaptation to the different materials and wetting conditions.

DISCUSSION

As expected, wetted materials had higher bacterial and fungal growth rates and were dominated by a few particular microbes, most notably the bacterial genera *Bacillus*, *Erwinia,* and *Pseudomonas* and the fungal genera *Eurotium* and *Penicillium*. This dominance led to an overall lower alpha diversity compared to non-wetted tiles. Wetting condition and material type described the majority of the variance in bacterial, fungal and metabolite structure. Interestingly, each wetted material showed its own unique microbe-metabolite dynamics.

Gypsum and MF gypsum were mostly colonized by *Bacillus*, with gypsum being a less selective environment, which allowed for several bacterial species to thrive on the same coupon simultaneously, each of them with high relative abundance and apparently sharing both the physical space and resources. In contrast, MF gypsum prevented most fungal growth and allowed *Bacillus* to dominate with little competition. MDF selected for fungal growth primarily, which allowed for the rapid accumulation of the antibacterial chemical, nigragillin, which is known to be made by the *Aspergillus* fungi. On OSB material, nigragillin and fumigaclavine C, a second fungal-synthesized antibacterial metabolite, may play important roles in microbial growth dynamics. Nigragillin, Fumigaclavine C, and *Aspergillus* relative abundance each gradually increases over time, whereas the abundance of *Pseudomonas* declines after the antibacterial

metabolites reach peak abundance, suggesting a dose dependent response **(Figure S11)**. These observations bolster our hypothesis that production of antibacterial metabolites by *Aspergillus* may inhibit the proliferation of surrounding bacteria. Also, there is a human health risk associated with the proliferation of the *Aspergillus* fungi in the BE. While the most common species identified in our data was *Aspergillus penicillioides,* a common indoor fungus in damp buildings with known associations to allergies and asthma (Edwards *et al.*, 2012, Hay *et al*., 1992), other *Aspergillus* species are known to be able to produce mycotoxins (including aflatoxins), molecules that have been associated with cancer and immunosuppression on humans (Roze *et al.,* 2013).

MOLD-RESISTANT GYPSUM

Traditional wood-based building materials contain natural polymers such as cellulose and lignin that are susceptible to degradation by fungal colonization (Gravesen *et al.*, 1999, Pasanen *et al.*, 1992). With some fungi having been shown to produce mycotoxins including aflatoxins that could affect human health (Roze *et al.*, 2013, Rand *et al*., 2017), building materials such as mold-resistant gypsum have been developed, which contain antifungal compounds intended to discourage fungal growth. We were particularly interested to examine the microbial communities on these surfaces and as expected, found that fungal growth was diminished on MF-gypsum compared to other materials. However, it appeared that the scarcity of fungal colonies made way for bacterial species to flourish with less competition; on non-wetted materials we observed MF-gypsum bacterial particle counts greater than on the other three materials, and on wetted materials while the MF-gypsum bacterial counts were second to MDF, the abundance level between non-wetted and wetted tiles, unlike MDF, remained minimally changed. This raises the potential that pathogenic bacteria colonization could occur on MF-gypsum and if wetted could grow and lead to negative health outcomes. In terms of metabolite production, thiabendazole and azoxystrobin were some of the anti-fungal compounds found in high abundance and overall a similar subset of compounds accounted for most of the metabolite abundance on this material, indicating lower metabolic diversity when the colonization is dominated by bacterial growth. We also detected a correlation between thiabendazole and *Penicillium*, which suggested the persistence of thiabendazole-resistant fungal strains.

DIVERSITY AND INTERACTION BETWEEN MICROBES AND ENVIRONMENT

Additionally, certain lipid metabolites (indicative of biofilm formation) showed significant positive correlation with both *Bacillus* and *Pseudomonas* OTUs, and these lipids were negatively correlated with the abundance of chloroplast OTUs, indicating that when bacteria and metabolites indicative of biofilm formation are detected in greater abundance, we see a proportional reduction in plant-associated signal. Similar to the lipids, metabolites annotated to organic molecules and vitamins were also negatively correlated with the chloroplast OTUs, which suggests that bacterial growth, indicated by increased proportion of 16S, cellular counts and associated metabolites, tends to swamp out the background material-chloroplast signal. We hypothesize that this may be because these molecules are being produced by bacteria colonizing and forming biofilms on the woody material. When the relative abundance of the bacteria increases, it reduces our ability to detect chloroplast sequences (based on a given sequencing depth); as such this negative correlation is likely due to the increased abundance of the microbes that mediate the production of these

metabolites, reducing the detection frequency of specific chloroplast OTUs, and not due to some mechanistic relationship between the wood and these molecules

MICROBIAL-METABOLITE INTERACTIONS.

Pseudomonads and Bacillus are often the main contributors to biofilm formation on material surfaces in the built environment (Ronan *et al.*, 2013; Powers *et al.*, 2015; Raaijmakers *et al.*, 2010). Biofilms are complex extracellular matrices formed by bacteria through the excretion of lipopeptide biosurfactants, to provide attachment to a surface to support colocalization with a nutrient source and protection from dehydration and chemical activity. Some of these lipopeptide biosurfactants produced by *Pseudomonas* and *Bacillus* species have been shown to have lytic or growth-inhibitory activity against many microorganisms such as bacteria, viruses, mycoplasmas, and fungi (Raaijmakers *et al.*, 2010). Powers *et al.* demonstrated that *Pseudomonas protegens* produces antibiotics that inhibit biofilm formation and sporulation in *Bacillus subtilis*. They also found that *Pseudomonas putida* secretes an unknown inhibitory compound that prevented biofilm-associated gene expression. In our study we demonstrate a number of compounds known to have potential biofilm inhibitory qualities that also co-correlate with either *Pseudomonas* or *Bacillus* abundance, suggesting potential competitive activity between these organisms. While *Pseudomonas–Bacillus* interactions have been shown to be competitive, interspecies interactions within the genus *Bacillus* are also important in the formation of biofilms, lipids like hydroxy fatty acids and mono-acyl-glycerophosphocholines could be building blocks or residual products of the biofilm creation (Shank *et al.*, 2011, Diomande *et al*., 2015, Dubois-Brissonnet *et al.*, 2016).

CONCLUSION

The simultaneous collection of environmental, metabolomic and microbial profiles reveals insights into the chemical signals that may govern BE microbial communities under high humidity conditions, as well as providing evidence that these the membership compete for space and resources. Here we show that wetting condition can profoundly alter both fungal and bacterial community succession, and that the taxa which dominate samples after wetting or exposure to high humidity are not abundant in non-wetted materials and have little relation to the skin-associated taxa which dominate samples of indoor environments. After wetting, the microbial community undergoes a successional trajectory that can result in similar metabolic diversity even when taxonomic diversity remains variable. We further show that while material choice significantly influences bacterial diversity, the same is not true of fungal diversity. In summary, BE microbial ecology once seen as a wasteland (Gibbons, 2016) could rather be seen as a desert environment mostly formed with smaller assemblages that can rapidly become an active ecologically dynamic community if water, in liquid or vapor form, is added. When a material experience high moisture conditions, both fungal and bacterial growth rapidly accelerate and the metabolites associated with their adaptation to different surface materials and competition for resources demonstrate ready made eco-evolutionary adaptation to this sporadic availability of a crucial resource; this phenomenon is very similar to what has been observed in real desert soil microbiomes (Neilson *et al.*, 2017), as well as in very different ecosystems, such as sediments exposed to oil pollution (Handley *et al.*, 2017).

Methods

Test materials

Four building materials were used in this study: oriented strand board (OSB), medium density fiberboard (MDF), regular gypsum wallboard, and mold-resistant (i.e., mold-free, or 'MF') gypsum wallboard. All samples were purchased new from a home improvement store in Chicago, IL. The building materials were cut into 5 cm × 5 cm coupons for testing. The material coupons were sterilized by UV irradiation for 20 minutes followed by surface cleaning with a 70% ethanol solution.

Inoculation

The building material coupons were naturally inoculated by placing them uncovered on the floor inside two residences for a period of approximately 50 days each. The goal was to allow for natural settling of microbes from each indoor environment onto the material surfaces. Another set of test coupons was covered with aluminum foil and kept in the laboratory for the same duration to be used as a control group. Each set of test coupons included 44 coupons for each type of building material (i.e., 176 coupons in total) to allow for multiple subsequent sampling strategies. One set of test coupons was placed inside a 6th floor apartment unit with two adult occupants and a medium sized dog located in downtown Chicago, IL (Location 1). The other set of materials was placed inside a 2-story single-family residence without any pets near the main campus of Illinois Institute of Technology, approximately 8 km south of the downtown residence (Location 2). During the inoculation periods, built environment metadata (Ramos & Stephens 2014) were collected in each residence, including temperature (T) and relative humidity (RH) using Onset HOBO U12 data loggers and occupant presence within ~1 m range of the samples using Onset UX90 data loggers. Coupons at a third location (the Built Environment Research Laboratory at the of Illinois Institute of Technology) were covered with aluminum foil to minimize natural inoculation, serving as a control group.

Wetting and incubation

After inoculation, half of each set of materials (i.e., 22 coupons each) from each location, as well as 22 coupons from the control group, were submerged in sterilized tap water in separate pans for ~12 hours to simulate the process of wetting of building materials due to a flood or leak. The other half of each set of materials (i.e., the other 22 coupons each) from each location and the other 22 coupons from the control group were not submerged in water. Next, to encourage fungal growth on all of the building materials, all of the material coupons were placed in trays (each tray contained all 22 coupons of one type of material from one location or control group) and were incubated at room temperature (24 ± 2.7°C) inside a static airtight chamber (0.9 m × 1.2 m × 0.4 m). Salt solutions (potassium nitrate) were used to maintain high RH near ~94% for the duration of the experiment. Temperature and RH in the chamber were also recorded using Onset HOBO U12 data loggers.

Sampling procedures

The material coupons were sampled for off-line biological and chemical analysis at 7 different

sampling time points, referred to here as: TP0, TP1, TP2, TP3, TP4, TP5, and TP6. The initial samples (TP0) were taken just after retrieving the samples from the field inoculation and represent non-wetted, naturally inoculated samples previously held at normal residential humidity conditions. The remaining sampling time points occurred every ~5 days. At each time point, a new coupon of each material from each condition that had never been swabbed before was swabbed, while duplicates of previously un-swabbed samples were also swabbed periodically (at TP0, TP2, TP4, and TP6) for comparison. Two samples ('TP0' and 'TP0 duplicated') were also swabbed at every time point to investigate whether repeatedly swabbing the surfaces impacted the results. Duplicates of both previously swabbed and previously un-swabbed samples were also included to investigate whether or not natural inoculation and subsequent growth was evenly distributed across multiple coupons. **Figure S1** illustrates the experimental setup and **Figure S14** shows coupons' photographs at TP5 and TP6 for each one of the three locations. Details of swabbing procedure at each time point are described below.

First, sampling reagents were prepared as follows. Phosphate-buffered saline (PBS) was used for microbial samples that were to be analyzed for DNA and formaldehyde was used for microbial samples that were to be analyzed by microscopy. For PBS, 500 µl 1X PBS was added to 1.7 ml microtubes for each sample to be collected. For formaldehyde, 100 µl 4% paraformaldehyde was added to 1.7 ml microtubes for each sample. Microcentrifuge tubes were filled with ethanol solution (200 µl 50% EtOH) to preserve samples for surface chemistry/metabolomics analysis.

For subsequent DNA sequencing and analysis, the entire surface of the test coupons was swabbed using two BD Screw Cap SWUBETM Polyester swabs for approximately 20 sec. The same researcher swabbed every time to keep the swabbing process consistent. One of the double swabs was placed into the tube with PBS and frozen for shipping for subsequent sequencing. The tip of the other of the double swabs was placed into microtubes and the swab tips were vortexed for 10 seconds. 100 µL of sample buffer was removed added to the tube containing 100 µL 4% paraformaldehyde for fixation. These fixed samples were stored in a refrigerator at 4°C and then sent to the San Diego State University team for running numerical counts of cells and virus particles using microscopy.

For surface and microbial chemistry analysis (i.e., metabolomics), another test coupon was swabbed using a cotton-tipped applicator that is dipped in ethanol (Petras *et al.*, 2016). The end of the swabs were cut directly into pre-prepared collection tubes, stored at 4℃ for 2-3 hours, and then stored at -20℃ overnight. Swabs were then removed with clean forceps the next morning, then re-sealed into the microcentrifuge tubes and sent to the Northwestern University team on ice at -20℃ or lower. Overhead photos of each tray of coupons were also taken at each time point for image analysis using ImageJ to calculate the percentage of visible microbial growth coverage (Hoang et al. 2010).

Viral-like particle and bacterial microscopy counts

Epifluorescence microscopy was used to ensure that all samples contained bacteria and virus-like particles and to estimate their abundance. 100 µL of the paraformaldehyde-fixed samples were resuspended into 5 mL of sterile 0.02 µm filtered water. Each suspended sample was then filtered onto a 0.02 µm Whatman Anodisc filter membrane (Thurber et al., 2009). The filters were stained with 1X SYBR Gold and incubated for 10 minutes in the dark. Each filter was washed and mounted

553 onto slides to be observed. Visualization was performed using a QImaging Retiga EXi Fast Cooled
554 Mono 12-bit microscope and Image-Pro Plus software was used to collect digital images and
555 estimate VLP and bacterial abundances.

556 *Metabolomics analysis*

557 Samples were analyzed by High-Performance Liquid Chromatography and High-Resolution Mass
558 Spectrometry and Tandem Mass Spectrometry (HPLC-MS/MS). Specifically, the system
559 consisted of a Thermo Q-Exactive in line with an electrospray source and an Agilent 1200 series
560 HPLC stack including a binary pump, degasser, and autosampler, outfitted with a column (Waters
561 XBridge BEH Shield RP18, 100x2.1 mm, 5µm particle size with matching guard). The mobile
562 phase A was H_2O with 0.1% Formic Acid; B was Acetonitrile with 0.1% Formic Acid. The
563 gradient was as follows: 0-0.5 min, 98% A; 5 min, 80% A; 10-10.5 min, 5% A; 10.6-15 min, 98%
564 A, with a flow rate of 400 µL/min. The capillary of the ESI source was set to 275 °C, with sheath
565 gas at 40 arbitrary units and the spray voltage at 4.0 kV. In positive polarity mode, MS1 data was
566 collected at a resolution of 35,000. The precursor ions were subsequently fragmented using the
567 higher energy collisional dissociation (HCD) cell set to 30% normalized collision energy in MS2
568 at a resolution power of 17,500. Data were processed with Compound Discoverer 2.0 (Thermo
569 Fisher) with MS/MS metabolite identifications made by comparing experimental MS/MS spectra
570 with library spectra from MZCloud (lower cutoff score of 90% match).
571
572 For the metabolites that were selected for more in-depth characterization, classification of structure
573 or substructure was performed by searching databases such as the Dictionary of Natural Products,
574 the LIPID MAPS Structure Database, and GNPS (Global Natural Products Social Molecular
575 Networking). Predicted structures resulting from a matched intact mass (≤10 ppm error) were
576 subsequently validated through manual analysis of fragmentation mass spectra.
577
578 Metabolite differential abundances (fold calculations) were calculated from Compound Discoverer
579 median peak areas for each compound including all three sampled locations.
580
581 *DNA extraction and sequencing*

582 To perform DNA extraction, the Qiagen DNeasy Powersoil HTP kit was used with a modified
583 protocol optimized for low-biomass samples. Swab tips were inserted into each well of the bead
584 plate, and then cut off using a sterilized wire cutter. The manufacturer's protocol was then
585 followed, with the following modifications: before cell lysis, the bead plates (containing beads,
586 bead solution, swabs, and the C1 solution) were heated for 20 minutes at 60°C in a water bath.
587 Additionally, the protocol steps using solutions C2 and C3 were combined into a single step, by
588 adding 150 µl each of C2 and C3 together to the lysed sample in the 1 ml plate.

589 The DNA obtained from the DNA extraction was used for both high-throughput 16S/ITS
590 sequencing, and qPCR. The 16S sequencing targeted the V4 region of the bacterial 16S rRNA
591 gene, using the primer pairs 515F/806R. The ITS sequencing targeted the highly variable fungal
592 internal transcribed spacer region located between the 5.8S and 18S rRNA genes. Both primer sets
593 used the same reaction mix and thermocycler instructions: Reaction mix: 9.5 µL of molecular
594 biology grade H_2O, 12.5 µL of Accustart II PCR Toughmix, 1 µL each of forward and reverse
595 primers at 5 µM, and 1 µL of sample DNA for a total reaction volume of 25 µL.

To make both the 16S and ITS amplicons, the following PCR program was used: Initial denaturing step at 94°C for 3 minutes, followed by 35 cycle of: 94°C for 45 seconds, 50°C for 60 seconds, and 72°C for 90 seconds, followed by a final extension step of 72°C for 10 minutes. The resulting amplicons were quantified using the Picogreen dsDNA binding fluorescent dye on a Tecan Infinity M200 Pro plate reader and pooled to 70 ng DNA per sample using the Eppendorf epMotion 5075 liquid handling robot. Primers and PCR reagents were removed using Agencourt AMPure beads, and then the clean amplicon pool was sequenced at Argonne National Laboratory's Environmental Sample Preparation and Sequencing Facility, following the Earth Microbiome Protocol (Caporaso *et al.,* 2011). Sequencing was performed on an Illumina Miseq using V3 chemistry, generating 2x150nt reads.

qPCR was performed using a Roche LightCycler 480 II. The 515F/806R primer pair was used again for amplification, using a mix of 10 µL Light Cycler 480 SYBR Green I Master mix, 6 µL of molecular biology grade H_2O, 1 µL of 515F primer (10 µM), 1 µL of 806R primer (10 µM), and 2 µL of template DNA for a total of 20 µL per reaction. The following thermocycler conditions were used: (1) 95°C for 5 minutes, (2) 95°C for 10 seconds, (3) 45°C for 45 seconds, (4) Measure fluorescence, with steps 2 through 4 repeated 50 times. To determine the copy number of the 16S gene (and therefore the number of organisms per swab), a standard curve was generated using a serial dilution of a plasmid containing the *E. coli* 16S rRNA gene.

Treatment of Technical Replicates

We used Mantel test to determine whether the bacterial communities on replicate tiles (tiles on the same tray sampled at the same time) significantly resembled each other and preserved patterns of beta-diversity. We began by calculating the Bray-Curtis dissimilarity between each pair of samples taken from the same tile type using the *beta_diversity.py* function from the software QIIME 1.9.1 (Caporaso *et al.*, 2010), producing dissimilarity matrices for each sampling type. Then the Mantel test and false discovery rate adjustment was performed using the *mantel* and *p.adjust* functions in the Vegan and stats R packages. For all comparisons between the sampling types the mantel statistic (which measures the stress in the fit of the two matrices) was significantly high (mantel >= 0.67 for fungi and >= 0.5 bacteria (all $p < 1E-05$) (**Table S2** (Fungi) **and S3** (Bacteria)). Based on the highly significant resemblance between tile types, we treated all samples of the same type as technical replicates, meaning that all combinations of material, location, wetting condition, and time point had either 2 (time point 0), 3 (time points 1, 3, and 5), or 4 (time points 2, 4, and 6) replicates.

Rarefaction and statistical analyses

After sequencing and sample merging, bacterial and Fungi OTU tables were rarefied to 1,000 and 10,000 reads respectively for statistical analyses. Rarefaction and statistical analyses were performed using R.

Random forest analyses

Random forest models were implemented using the "randomForest" R package. Samples from timepoint 0 were removed from the dataset. Models were built with 1000 trees and 10-fold cross

636 validation. For each of the 10 models for each metadata criterion, a randomly drawn 70% of
637 samples (100 samples) were used for model training and the remaining 30% (44 samples) were
638 used for validation.

639 *NMDS*

640 We visualized sample similarity using non-metric multi-dimensional scaling (NMDS) ordination
641 based on Bray-Curtis dissimilarity. Metadata vectors were fit onto the ordination using the *envfit*
642 command in the Vegan R package. We converted material, location, and wetting condition into
643 dummy variables (1 = yes, 0 = no) and, in the case of the bacterial and fungal datasets; also fit
644 vectors of relative abundance for the common genera described in **Figure 3**. We assessed
645 significance of each of the vectors using 10^5 permutations, and removed non-significant vectors
646 from the figure. The R^2 values for each vector and their significance is presented in **Table S1**

647 *Co-occurrence networks*

648 Traditional correlation networks are unsuited to genomic survey data as these data are relative,
649 rather than absolute, measures of community composition. Since the relative abundances of all
650 taxa within each sample must sum to 1, the fractions are not independent and will often exhibit
651 negative correlations to each other regardless of the true correlation in absolute abundance. To
652 avoid these compositional effects, we generated our networks using SparCC (Friedman & Alm,
653 2012), a correlation metric based on log-ratio transformed data that is specifically suited to
654 compositional genomic surveys. Pseudo-p values for each correlation were generated through
655 comparison from 100 to 1,000 bootstraps of the permuted OTU table.

656 For the same kingdom and microbe-metabolite networks only samples where either bacteria or
657 fungi and metabolites were found in detectable levels after rarefaction were used (N=83, N= 91
658 respectively). Additionally, only bacterial OTUs with >9 reads, fungi OTUs with >99 reads, and
659 metabolites with > 5'000,000 abundance in the rarified dataset were used for a total number of 630
660 bacterial OTUs, 352 fungi OTUs and 426 metabolites. Figures were generated using CAVNet R
661 package (Cardona, 2017) and only displayed the higher correlation threshold (positive or negative)
662 greater than 0.4.

663 For the network encompassing both bacteria and fungi, the OTUs reads threshold remained the
664 same but only samples with both 16S and ITS data were kept (N = 153) producing a new subset
665 of bacterial and fungi OTUs, 590 and 581 OTUs respectively. This dataset produced a co-
666 occurrence network with 1,171 nodes. Only positive correlations with a pseudo-p < 0.05 were
667 included, resulting in a network with 33,509 edges (density = 0.052). The network was ordinated
668 using the Fruchterman-Reingold Algorithm (edge-weighted, force-directed) in the *igraph* R
669 package, with node size based on the log read count of each OTU across all samples (with ITS
670 counts first divided by 10 to equalize rarefaction depth between datasets). We used the Walktrap
671 method (Pons & Latapy, 2005) to uncover dense subgraphs (modules) within the network, which
672 may correspond to distinct community structures. We chose Walktrap (which is based on random
673 walks within the network) as our method of community inference due to its computational
674 tractability and its accuracy at uncovering subgraphs regardless of network size (Yang *et al.*, 2016).
675 We used random walks of four steps, which resulted in four distinct modules with a network
676 modularity of 0.45

677

REFERENCES

678 Adams, Rachel I., et al. "Ten questions concerning the microbiomes of buildings." *Building and Environment* 109
679 (2016): 224-234.
680
681 Adams, Rachel I., et al. "Dispersal in microbes: fungi in indoor air are dominated by outdoor air and show dispersal
682 limitation at short distances." The ISME journal 7.7 (2013): 1262.
683
684 Balba, Hamdy. "Review of strobilurin fungicide chemicals." *Journal of Environmental Science and Health Part*
685 *B* 42.4 (2007): 441-451.
686
687 Caporaso, J. Gregory, et al. "Global patterns of 16S rRNA diversity at a depth of millions of sequences per
688 sample." *Proceedings of the national academy of sciences*108.Supplement 1 (2011): 4516-4522.
689
690 Caporaso, J. Gregory, et al. "QIIME allows analysis of high-throughput community sequencing data." *Nature*
691 *methods* 7.5 (2010): 335.
692
693 Cardona C. 2017. CAVNet: Creation Analysis and Visualization of Networks Package. Bitbucket.
694 https://bitbucket.org/JackGilbertLab/cavnet
695
696 Chase, John, et al. "Geography and location are the primary drivers of office microbiome
697 composition." *MSystems* 1.2 (2016): e00022-16.
698
699 Clausen, Carol A., and Vina Yang. "Protecting wood from mould, decay, and termites with multi-component
700 biocide systems." *International Biodeterioration & Biodegradation* 59.1 (2007): 20-24.
701
702 Cole, Richard J., et al. "Mycotoxins produced by Aspergillus fumigatus species isolated from molded
703 silage." *Journal of Agricultural and Food Chemistry* 25.4 (1977): 826-830.
704
705 Coombs, Kanistha, et al. "Fungal microbiomes associated with green and non-green building
706 materials." *International biodeterioration & biodegradation* 125 (2017): 251-257.
707
708 Dannemiller, Karen C., et al. "Combining real-time PCR and next-generation DNA sequencing to provide
709 quantitative comparisons of fungal aerosol populations." *Atmospheric environment* 84 (2014): 113-121.
710
711 Diomande, Sara Esther, et al. "Role of fatty acids in Bacillus environmental adaptation." *Frontiers in microbiology* 6
712 (2015): 813.
713
714 Dubois-Brissonnet, Florence, Elsa Trotier, and Romain Briandet. "The biofilm lifestyle involves an increase in
715 bacterial membrane saturated fatty acids." *Frontiers in microbiology* 7 (2016): 1673.
716
717 Edwards, Michael R., et al. "The microbiology of asthma." Nature Reviews Microbiology 10.7 (2012): 459.
718
719 Fisk, William J., Ekaterina A. Eliseeva, and Mark J. Mendell. "Association of residential dampness and mold with
720 respiratory tract infections and bronchitis: a meta-analysis." *Environmental Health* 9.1 (2010): 72.
721
722 Friedman, Jonathan, and Eric J. Alm. "Inferring correlation networks from genomic survey data." *PLoS*
723 *computational biology* 8.9 (2012): e1002687.
724
725 Gibbons, Sean M., et al. "Ecological succession and viability of human-associated microbiota on restroom
726 surfaces." *Applied and environmental microbiology* 81.2 (2015): 765-773.
727
728 Gibbons, Sean M. "The built environment is a microbial wasteland." *MSystems* 1.2 (2016): e00033-16.

Gnonlonfin, GJ Benoit, Ambaliou Sanni, and Leon Brimer. "Review scopoletin–a coumarin phytoalexin with medicinal properties." *Critical Reviews in Plant Sciences* 31.1 (2012): 47-56.
Gravesen, Suzanne, et al. "Microfungal contamination of damp buildings--examples of risk constructions and risk materials." *Environmental Health Perspectives* 107.Suppl 3 (1999): 505.

Handley, Kim M., et al. "Metabolic and spatio-taxonomic response of uncultivated seafloor bacteria following the Deepwater Horizon oil spill." *The ISME journal* 11.11 (2017): 2569.

Hay, D. B., B. J. Hart, and A. E. Douglas. "Evidence refuting the contribution of the fungus Aspergillus penicillioides to the allergenicity of the house dust mite Dermatophagoides pteronyssinus." *International archives of allergy and immunology 97.1* (1992): 86-88.

Hegarty, Bridget, K. C. Dannemiller, and Jordan Peccia. "Gene expression of indoor fungal communities under damp building conditions: Implications for human health." *Indoor air* (2018).

Herter, T., et al. "Glucose-1-phosphatase (AgpE) from Enterobacter cloacae displays enhanced phytase activity." *Applied microbiology and biotechnology* 70.1 (2006): 60-64.

Hoang, Chi P., et al. "Resistance of green building materials to fungal growth." *International Biodeterioration & Biodegradation*64.2 (2010): 104-113.

Holmes, Gerald J., and Joseph W. Eckert. "Sensitivity of *Penicillium digitatum* and *P. italicum* to postharvest citrus fungicides in California." *Phytopathology* 89.9 (1999): 716-721.

Hyvärinen, Anne, et al. "Fungi and actinobacteria in moisture-damaged building materials—concentrations and diversity." *International Biodeterioration & Biodegradation* 49.1 (2002): 27-37.

IAQ Report - Prevalence of Building Dampness Available at: https://iaqscience.lbl.gov/dampness-prevalence.

IAQ Report - Nature and Causes of Building Dampness Available at: https://iaqscience.lbl.gov/dampness-nature.

Institute of Medicine (US) Committee on Damp Indoor Spaces and Health. Damp Indoor Spaces and Health. Washington (DC): National Academies Press (US); 2004. Available from: https://www.ncbi.nlm.nih.gov/books/NBK215643/doi: 10.17226/11011

Isogai, Akira, et al. "Isolation and identification of Nigragillin as a insecticidal metabolite produced by a *Aspergillus niger*." *Agricultural and Biological Chemistry* 39.3 (1975): 739-740.

Jaakkola, Maritta S., et al. "Association of indoor dampness and molds with rhinitis risk: a systematic review and meta-analysis." *Journal of Allergy and Clinical Immunology* 132.5 (2013): 1099-1110.

Jensen, Peter Ø., et al. "Formation of hydroxyl radicals contributes to the bactericidal activity of ciprofloxacin against Pseudomonas aeruginosa biofilms." *Pathogens and disease*70.3 (2014): 440-443.

Johansson, Pernilla, et al. "Laboratory study to determine the critical moisture level for mould growth on building materials." *International Biodeterioration & Biodegradation* 73 (2012): 23-32.

Kong, Na-Na, et al. "Flavonoids from the halophyte Apocynum venetum and their antifouling activities against marine biofilm-derived bacteria." *Natural product research* 28.12 (2014): 928-931.

Lax, Simon, et al. "Longitudinal analysis of microbial interaction between humans and the indoor environment." *Science* 345.6200 (2014): 1048-1052.

Lax, Simon, et al. "Bacterial colonization and succession in a newly opened hospital." *Science translational medicine* 9.391 (2017): eaah6500.

Lerat, Sylvain, et al. "Streptomyces scabiei and its toxin thaxtomin A induce scopoletin biosynthesis in tobacco and Arabidopsis thaliana." *Plant cell reports* 28.12 (2009): 1895-1903.

Magdy, Wesam, et al. "Nigragillin, Nigerazine B and Five Naphtho-γ-pyrones from Aspergillus japonicus Isolated from Hot Desert Soil." *The Natural Products Journal* 7.3 (2017): 216-223.

Mendell, Mark J., et al. "Respiratory and allergic health effects of dampness, mold, and dampness-related agents: a review of the epidemiologic evidence." *Environmental health perspectives* 119.6 (2011): 748.

Mille-Lindblom, Cecilia, Helmut Fischer, and Lars J. Tranvik. "Antagonism between bacteria and fungi: substrate competition and a possible tradeoff between fungal growth and tolerance towards bacteria." *Oikos* 113.2 (2006): 233-242.

Miller, J. David, and David R. McMullin. "Fungal secondary metabolites as harmful indoor air contaminants: 10 years on." *Applied microbiology and biotechnology* 98.24 (2014): 9953-9966.

Nascimento, M. S., et al. "Phenolic extractives and natural resistance of wood." *Biodegradation-Life of Science*. InTech, 2013.

Neilson, Julia W., et al. "Significant Impacts of Increasing Aridity on the Arid Soil Microbiome." *MSystems* 2.3 (2017): e00195-16.

Pasanen, A-L., et al. "Occurrence and moisture requirements of microbial growth in building materials." *International Biodeterioration & Biodegradation* 30.4 (1992): 273-283.

Petras, Daniel, et al. "Mass spectrometry-based visualization of molecules associated with human habitats." *Analytical chemistry* 88.22 (2016): 10775-10784.

Pinheiro, Eduardo Antonio A., et al. "Antibacterial activity of alkaloids produced by endophytic fungus Aspergillus sp. EJC08 isolated from medical plant Bauhinia guianensis." *Natural product research* 27.18 (2013): 1633-1638.

Pons, Pascal, and Matthieu Latapy. "Computing communities in large networks using random walks." *International symposium on computer and information sciences*. Springer, Berlin, Heidelberg, 2005.

Powers, Matthew J., et al. "Inhibition of cell differentiation in Bacillus subtilis by *Pseudomonas protegens*." *Journal of bacteriology* (2015): JB-02535.

Quansah, Reginald, et al. "Residential dampness and molds and the risk of developing asthma: a systematic review and meta-analysis." *PloS one* 7.11 (2012): e47526.

Raaijmakers, Jos M., et al. "Natural functions of lipopeptides from Bacillus and Pseudomonas: more than surfactants and antibiotics." *FEMS microbiology reviews* 34.6 (2010): 1037-1062.

Rand, Thomas G., et al. "Inflammation-associated gene expression in RAW 264.7 macrophages induced by toxins from fungi common on damp building materials." *Toxicology in Vitro* 43 (2017): 16-20.

Ronan, Evan, et al. "Interspecies interaction extends bacterial survival at solid–air interfaces." *Biofouling* 29.9 (2013): 1087-1096.

Roze, Ludmila V., Sung-Yong Hong, and John E. Linz. "Aflatoxin biosynthesis: current frontiers." *Annual review of food science and technology* 4 (2013): 293-311

Shank, Elizabeth A., et al. "Interspecies interactions that result in Bacillus subtilis forming biofilms are mediated mainly by members of its own genus." *Proceedings of the National Academy of Sciences* (2011): 201103630.

Stephens, Brent. "What have we learned about the microbiomes of indoor environments?." *MSystems* 1.4 (2016): e00083-16.

Thurber, Rebecca V., et al. "Laboratory procedures to generate viral metagenomes." Nature protocols 4.4 (2009): 470.

Viitanen, Hannu, et al. "Moisture and bio-deterioration risk of building materials and structures." *Journal of Building Physics*33.3 (2010): 201-224.

Yang, Zhao, René Algesheimer, and Claudio J. Tessone. "A comparative analysis of community detection algorithms on artificial networks." *Scientific Reports* 6 (2016): 30750.

FIGURES

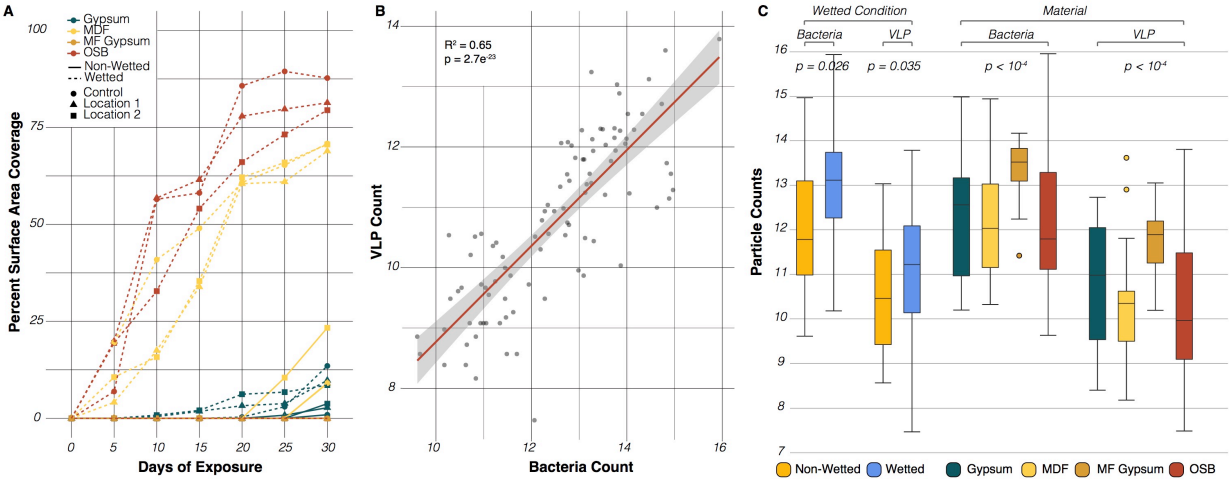

Figure 1: Microbial growth rates vary across sample types. (**A**) Percent of surface area covered by visible microbial growth through time (n=168, 4 materials, 3 locations, 2 wetting conditions, 7 time points). Color indicates tile material, point shape indicates inoculating location, and line type indicates whether the tile was wet before incubation. (**B**) Correlation in the counts of bacteria-like (BLP) and viral-like particles (VLP) across all tiles (n=96 samples, 4 materials, 3 locations, 2 wetting conditions, 4 time points). (**C**) Boxplots of BLP and VLP counts by wetting condition and by material (n=96 samples).

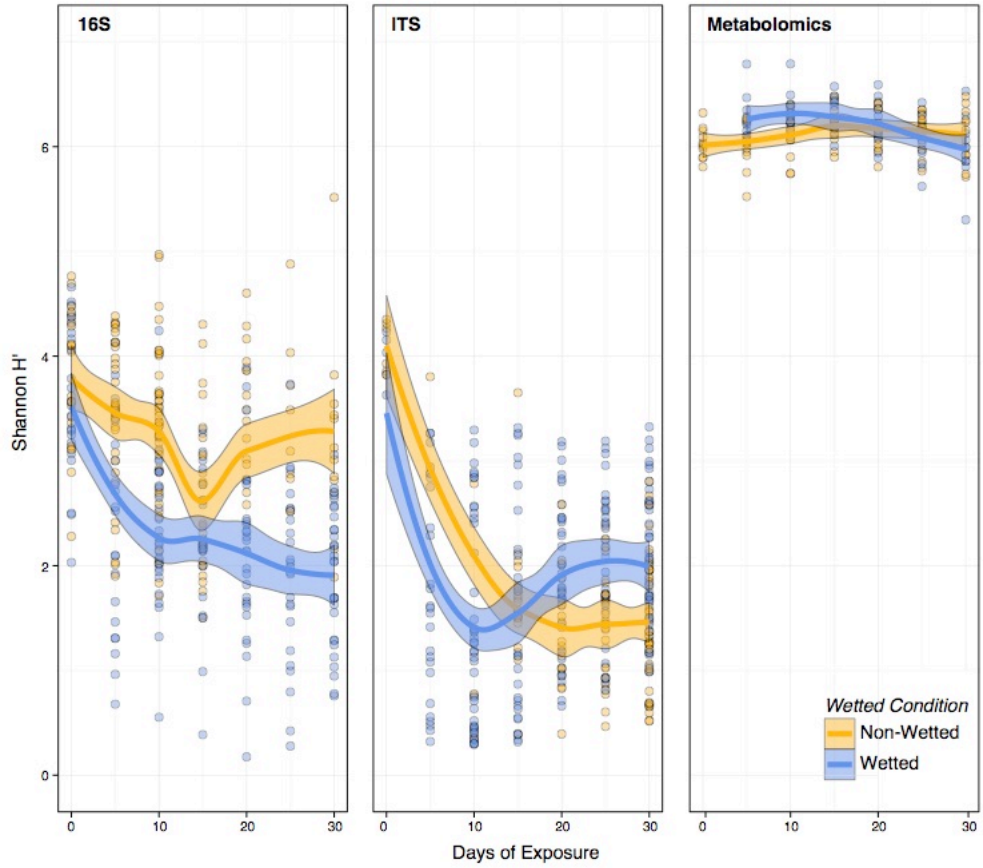

Figure 2: Change in the Shannon Index of samples over time. Points represent individual samples and the trend lines are a smoothed moving-average of the mean and shaded regions indicate the standard error (n=338, 330 and 144 samples for 16S, ITS and Metabolomics, respectively)

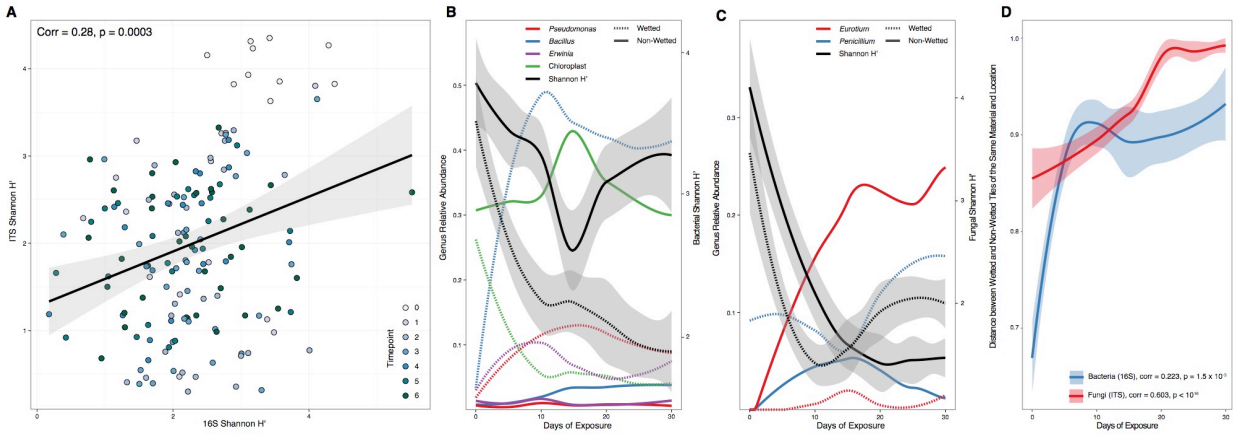

Figure 3: Overview of community succession. (**A**) Fungal diversity and bacterial diversity are significantly correlated across communities (n=153 samples). Points represent individual samples, colored by the time point at which the sample was taken. (**B**) Changes in the relative abundance of selected bacterial genera over the course of succession (n=338 samples). Lines represent a smoothed moving average of the mean. Genus is indicated by color and wetting condition is

indicted by line style. Average community diversity (Shannon H' at OTU level, as in Figure 3) is indicated by black lines with standard error indicated by the gray shaded region. Genus abundance is indicated on the left y-axis and Shannon H' is indicated on the right y-axis. (**C**) Changes in the relative abundance of selected fungal genera over the course of succession (n=330 samples). Formatting is as in (**B**). (**D**) Wet vs. non-wetted replicates of tiles of the same material and inoculating location become increasingly dissimilar over the course of community succession (n=338, 330 samples for 16S and ITS, respectively). The y-axis is the Bray-Curtis distance between replicates. Spearman correlation between community dissimilarity and time is indicated in the legend error

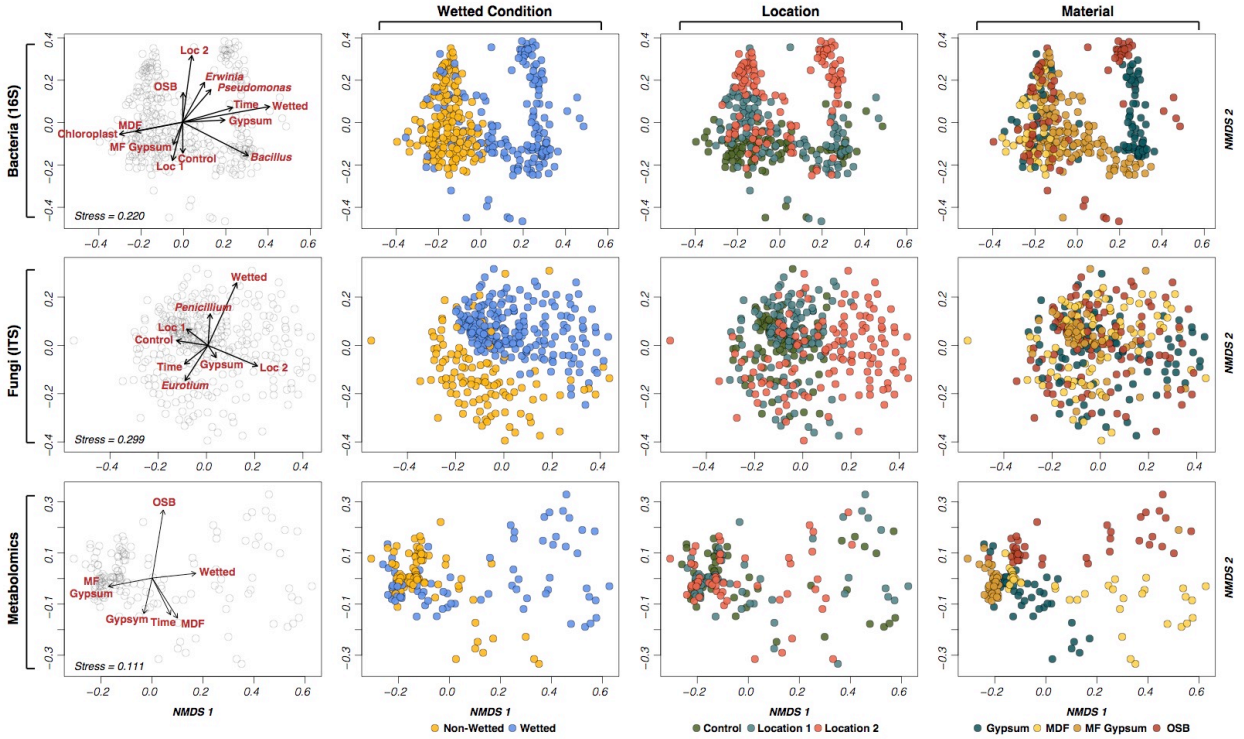

Figure 4: NMDS plots illustrate clustering of sample diversity by sample type. Each row comprises four identical NMDS plots (n=338, 330 and 144 samples for 16S, ITS and Metabolomics, respectively). The leftmost plot illustrates the ordination's association with environmental variables and the remaining plots color sample points by various metadata factors. The stress on the NMDS plot is indicated in the rightmost plot in each row error

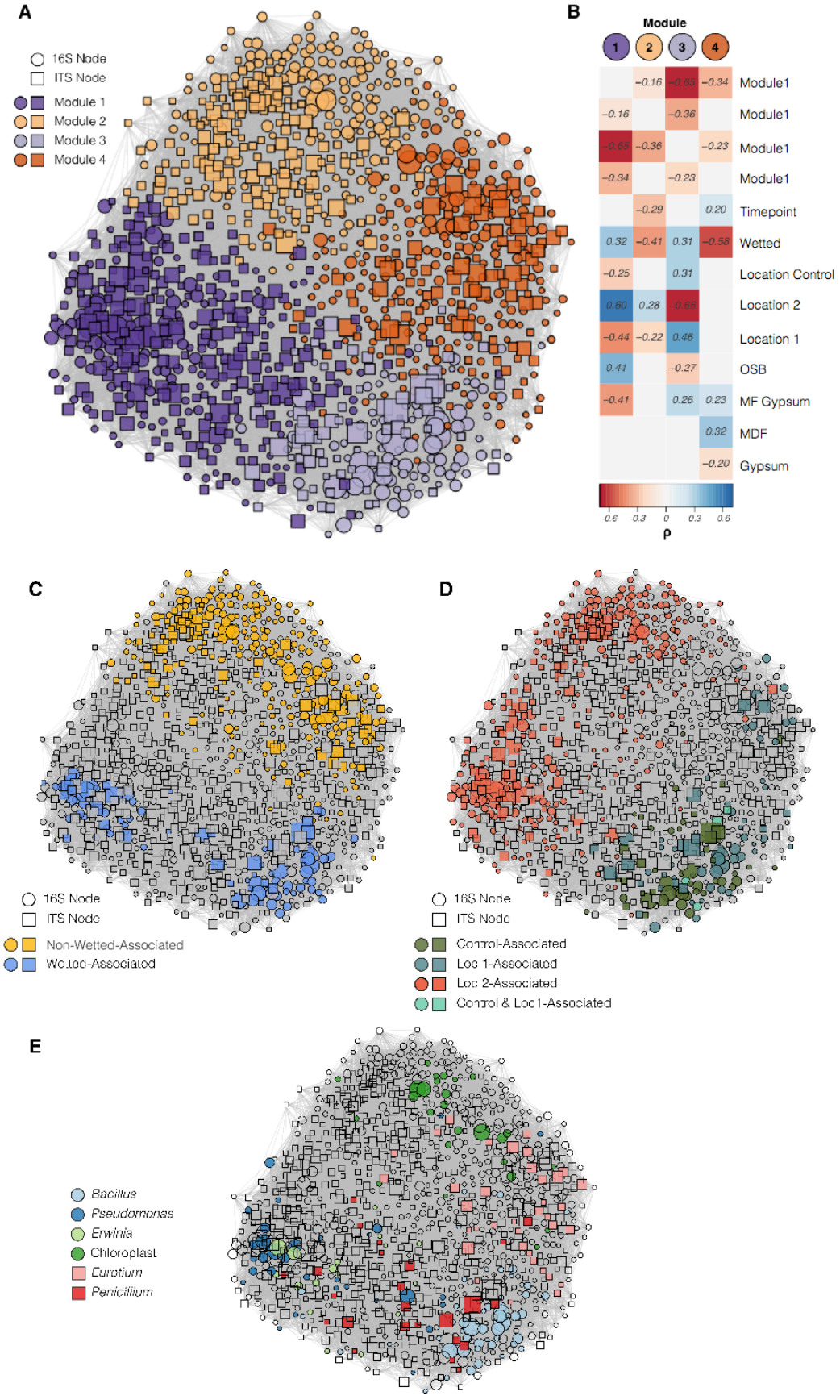

886 **Figure 5: Network of SparCC OTU correlations**. (**A**) Edge-weighted, spring-embedded
887 network ordination, with nodes colored by module membership. Node shape represents node type
888 (16S or ITS) and node size is based on the log-transformed abundance of each node (n=153 with
889 both 16S and ITS, respectively). (**B**) Correlations between metadata factors (treated as dummy
890 variables where true = 1 and false = 0) and the percent of reads in network modules. Non-
891 significant correlations are not shown. (**C**) Taxa enriched in wet or non-wetted samples, as
892 determined through a two-sided non-parametric t-test with 10^5 permutations. (**D**) Taxa enriched in
893 samples originating from an individual inoculating location, with statistical methods as in (**A**). (**E**)
894 Taxonomy of nodes in the genera included in Figure 4.

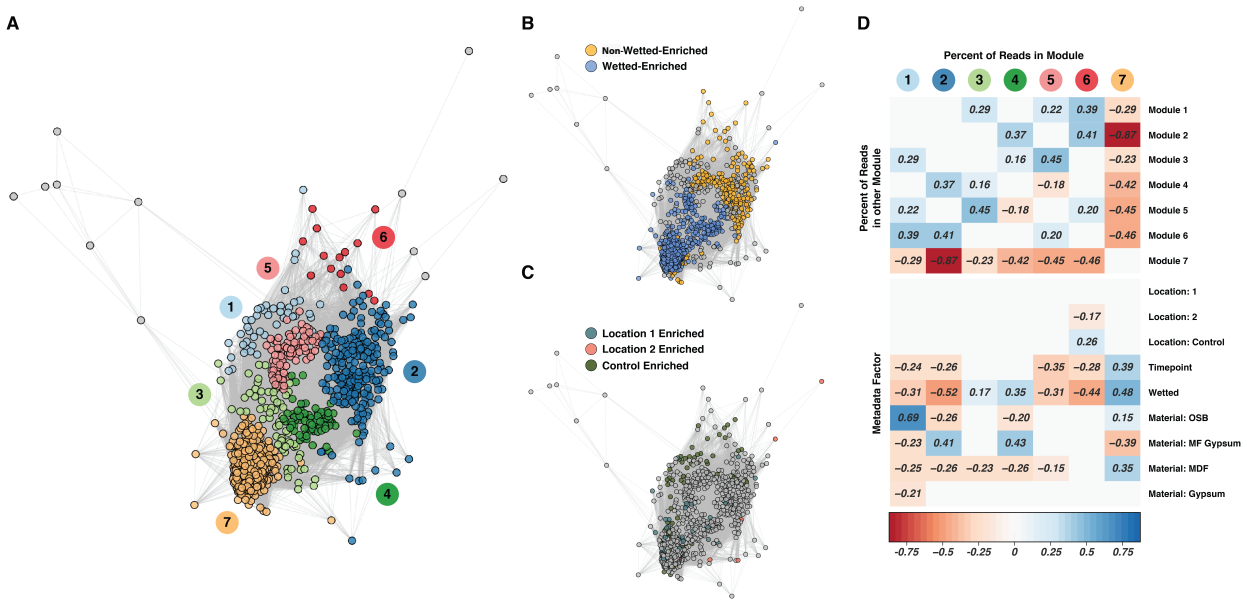

895 **Figure 6: Metabolite co-occurrence network**. (**A**) Network of significantly positive spearman
896 correlations between metabolites, with network module indicated by color (n=144 samples). (**B**)
897 Metabolites enriched in wet or non-wetted samples, as determined through a two-sided non-
898 parametric t-test with 10^5 permutations. (**B**) Metabolites enriched in samples originating from an
899 individual inoculating location, with statistical methods as in (**B**). (**C**) Correlations between
900 metadata factors (treated as dummy variables where true = 1 and false = 0) and the percent of
901 metabolites in network modules. Non-significant correlations are not shown.

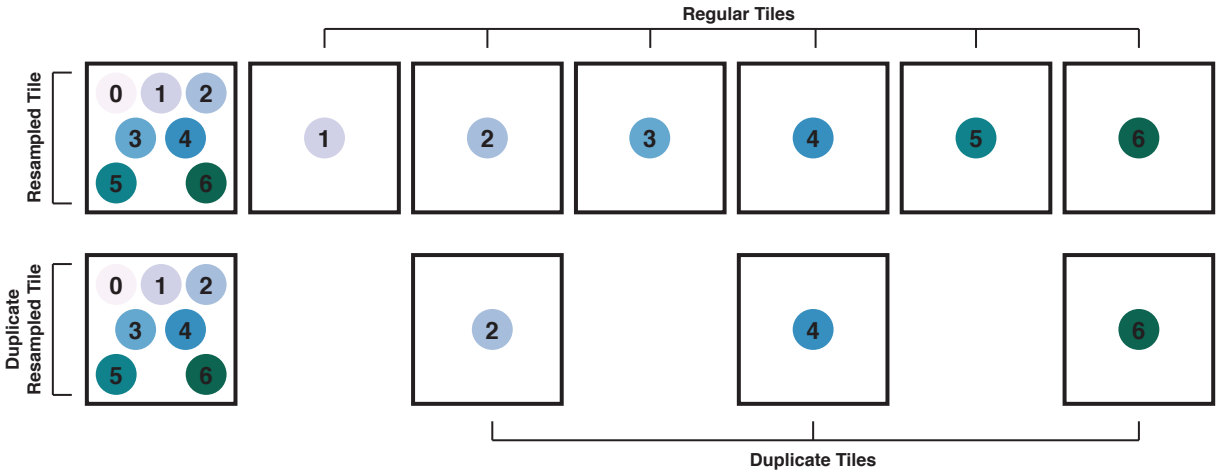

902 **Figure S1: Experimental setup of project.** Illustration of the experimental setup and coupon
903 sampling procedures**.**

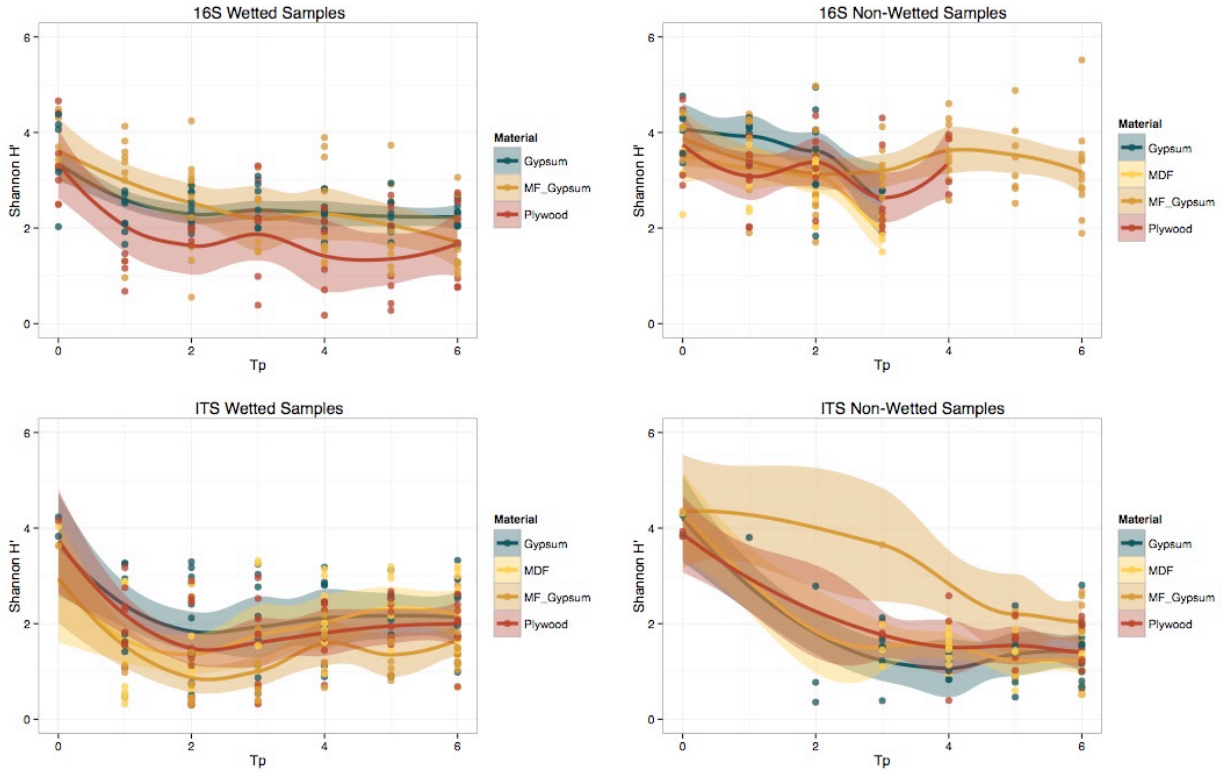

904 **Figure S2: Change in the Shannon Index by material over time.** Points represent individual
905 samples (n=338, 330 samples for 16S and ITS, respectively) and the trend lines are a smoothed
906 moving-average of the mean and shaded regions indicate the standard error
907

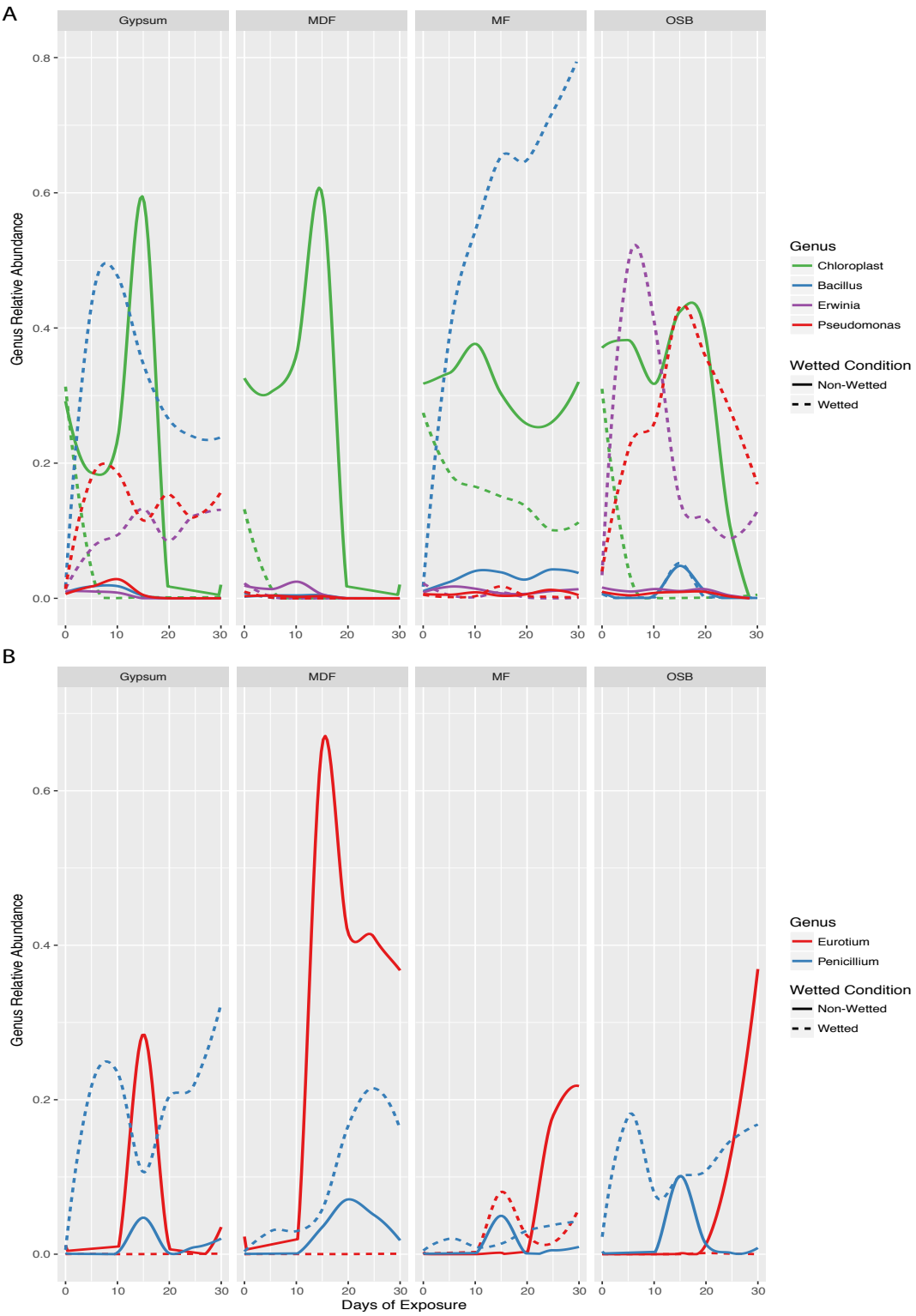

Figure S3: Microbial succession by material over time Changes in the relative abundance of selected microbial genera for each material over the course of succession. (n=338, 330 samples for 16S and ITS, respectively). (A) Lines represent a smoothed moving average of the mean. Genus

912 is indicated by color and wetting condition is indicted by line style. (**B**) Changes in the relative
913 abundance of selected fungal genera over the course of succession. Formatting is as in (**A**)
914
915

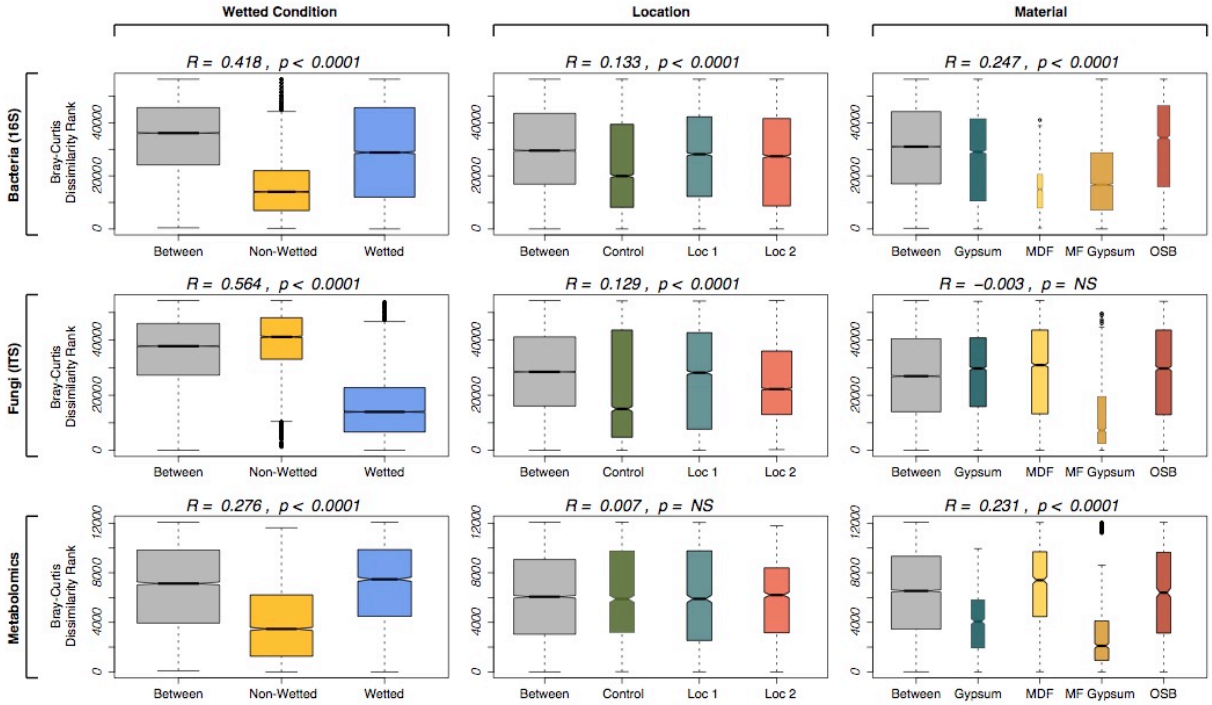

916 **Figure S4: ANOSIM quantifies the influence of metadata factors on the dissimilarity**
917 **between samples**. Columns represent different metadata factors and rows represent the three
918 datasets in this study (n=338, 330 samples for 16S and ITS, respectively). Boxplots depict the
919 range of ranked Bray-Curtis dissimilarities within and between factors (lower rank = lower
920 dissimilarity). Boxplot width indicates the number of samples represented by the boxplot
921

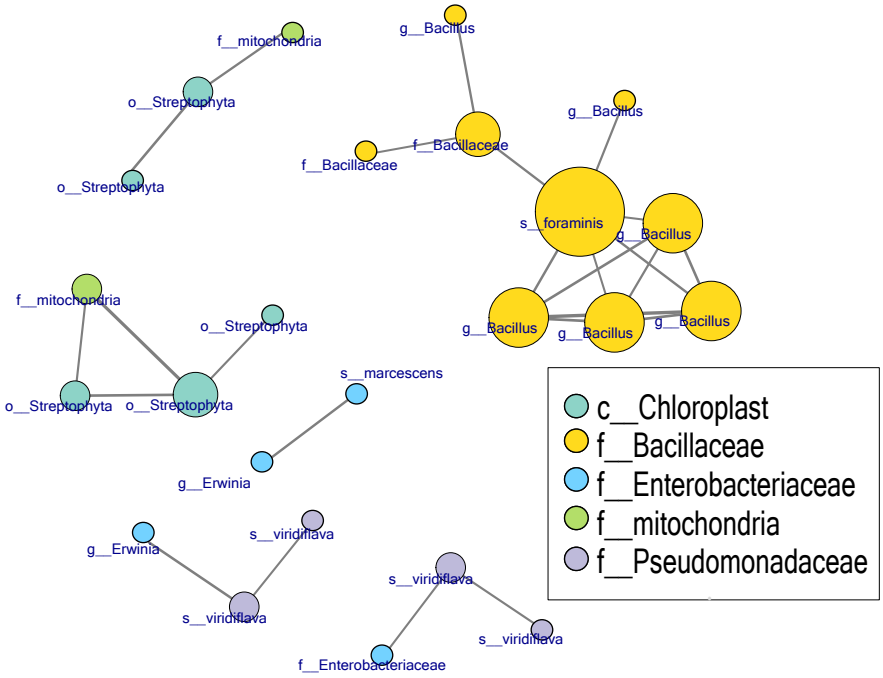

922 **Figure S5: Bacteria-Bacteria co-occurrence network.** Co-occurrence network (from n=83
923 bacteria samples) shows highly correlated bacteria form monophyletic clusters for samples
924 containing more abundant taxa
925

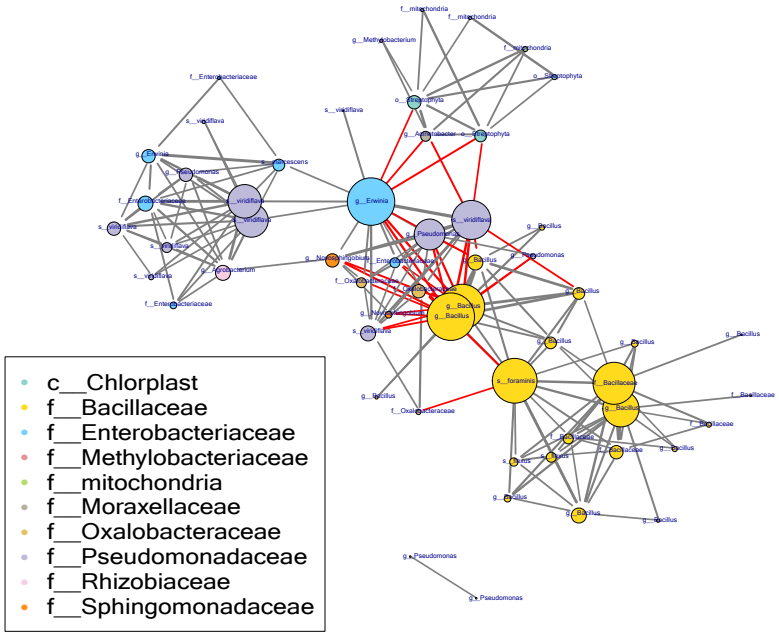

926
927 **Figure S6: Bacteria-Bacteria co-occurrence network on wet samples.** Co-occurrence network
928 (from n=39 wet samples) shows how *Pseudomonas* and *Bacillus* are anticorrelated on wet samples
929 for samples containing more abundant taxa
930
931

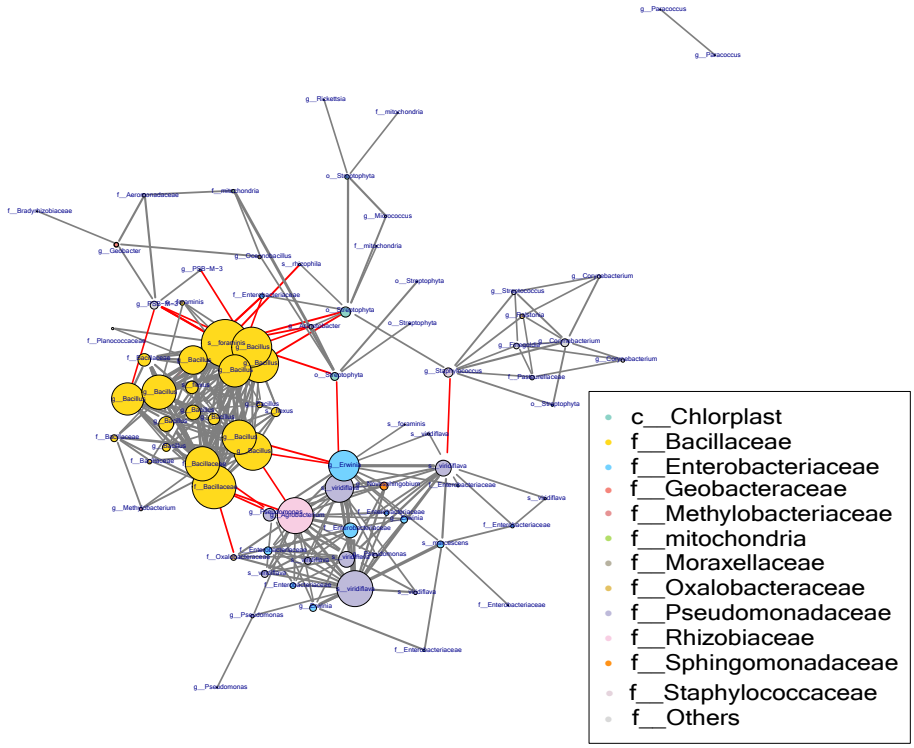

Figure S7: Bacteria-Bacteria co-occurrence network on gypsum samples. Co-occurrence network (from n=24 gypsum samples) shows how *Pseudomonas* and *Bacillus* are anticorrelated on all gypsum samples

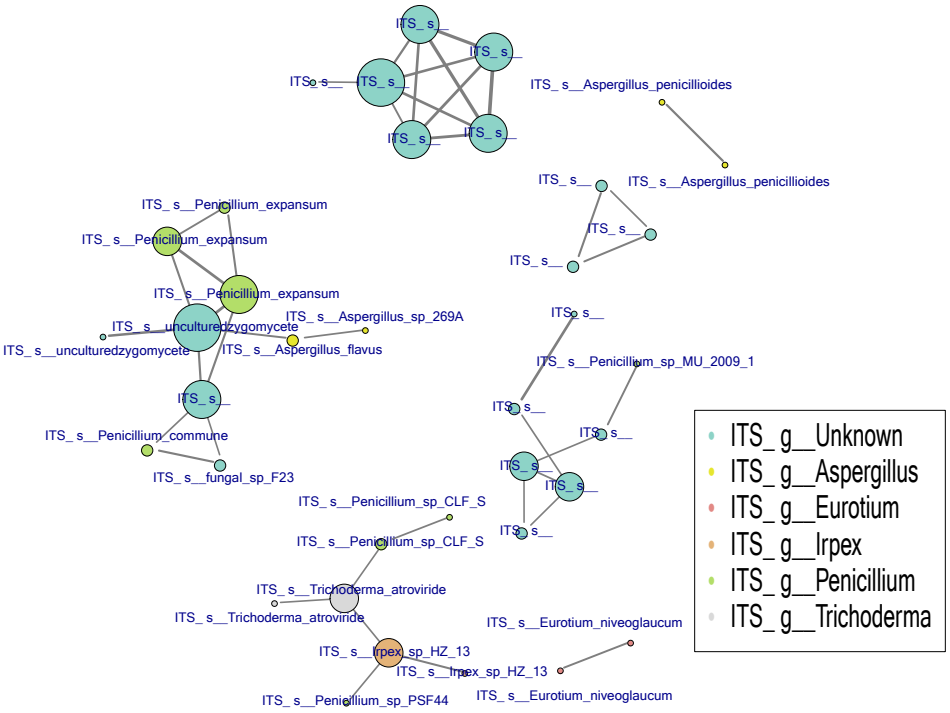

Figure S8: Fungi-Fungi co-occurrence network. Co-occurrence network (from n=91 fungi samples) shows highly correlated fungi forms mostly monophyletic clusters

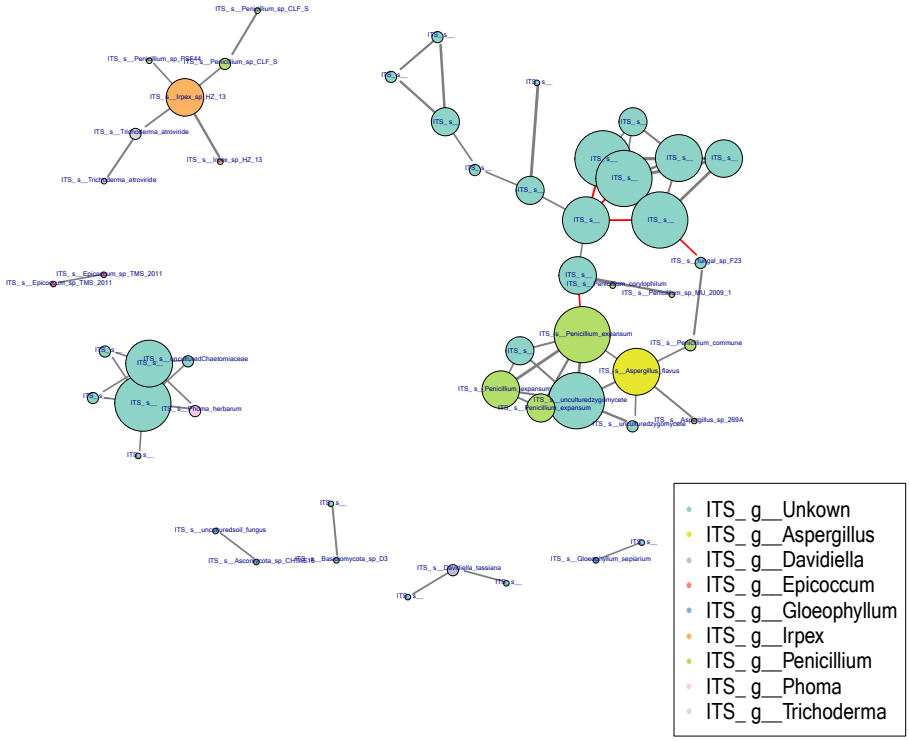

Figure S9: Fungi-Fungi co-occurrence network on wet samples. Co-occurrence network (from n=58 wet samples) shows how certain Fungi OTUs are anticorrelated on wet samples

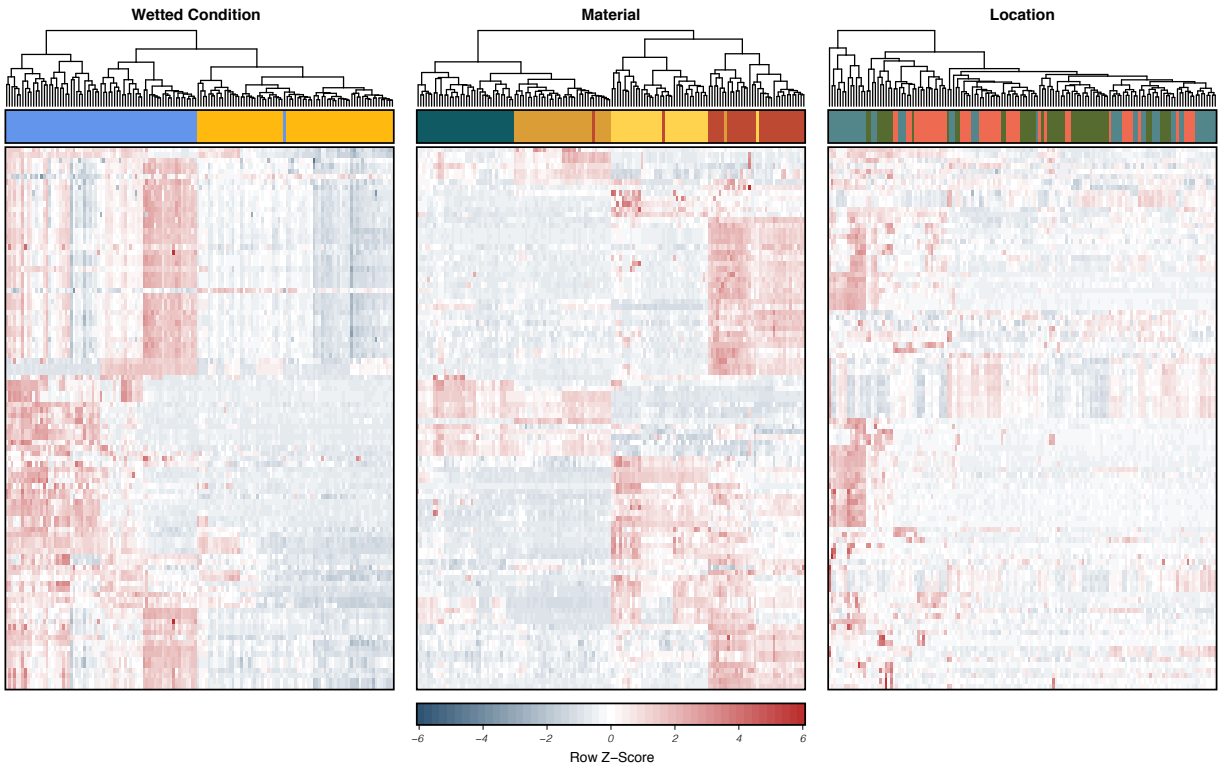

Figure S10: Random forest metabolite selection heatmap. Random forest learning was used to select the metabolites that most distinctly identify each environmental condition, wetted or non-wetted, wood material type and inoculation location (n=144 samples and 3187 metabolites), the 100 highest-scoring metabolite features for each condition where selected for further examination.

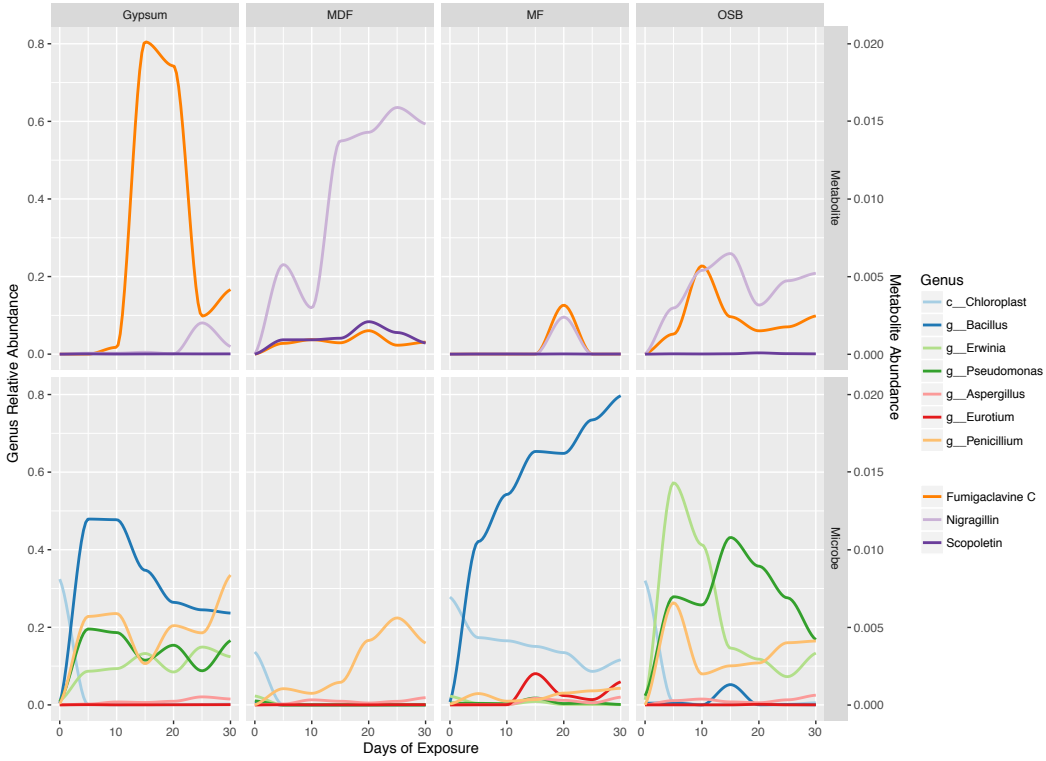

Figure S11: Metabolite and microbial succession on wet samples by material over time. Changes in the relative abundance of selected bacterial genera for each material over the course of succession (n=39, 58 and 72 wet samples for bacteria, fungi and metabolites, respectively). Lines represent a smoothed moving average of the mean. Genus and metabolites are indicated by different colors

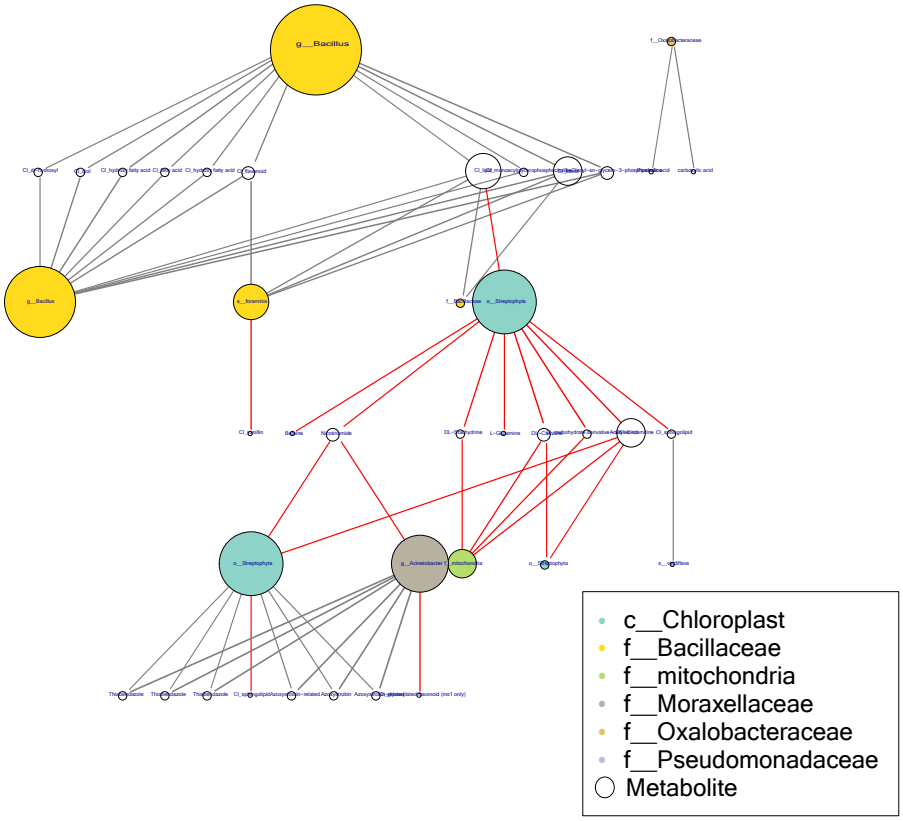

Figure S12: Bacteria-Metabolite co-occurrence network. Bacteria and Metabolite paired co-occurrences suggesting biochemical exchanges (from n=83, 144 samples, respectively). Lipid and hydroxyl compounds are strongly connected to *Bacillaceae* groups. Some specific lipids correlate positively with bacteria and negatively with wood material (plants). Vitamins and small carbon compounds negatively correlate with the wood material (plants).

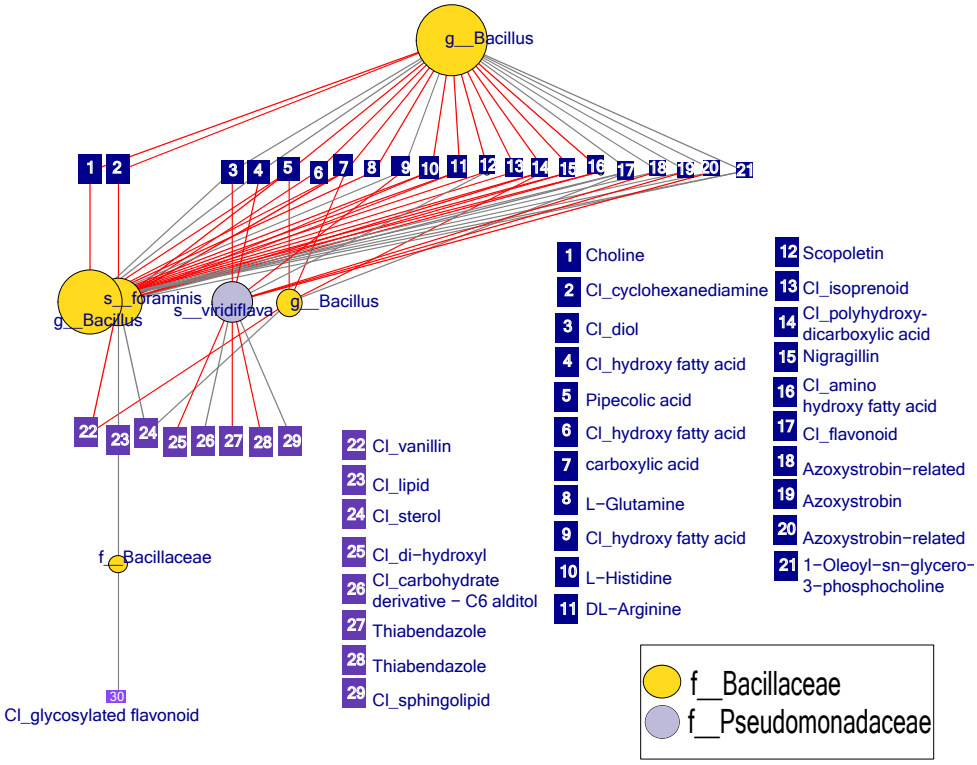

Figure S13: Bacteria-Metabolite co-occurrence network for Bacillus and Pseudomonas interactions only. Bacteria and Metabolite paired co-occurrences suggesting biochemical exchanges (from n=83, 144 samples, respectively). *Nigragillin* is negatively correlated with both *Pseudomonas* and *Bacillus. Azoxystrobin* correlates negatively with *Pseudomonas*, but positively with *Bacillus*. Hydroxyl compounds correlates negatively with *Pseudomonas* but positively with *Bacillus*

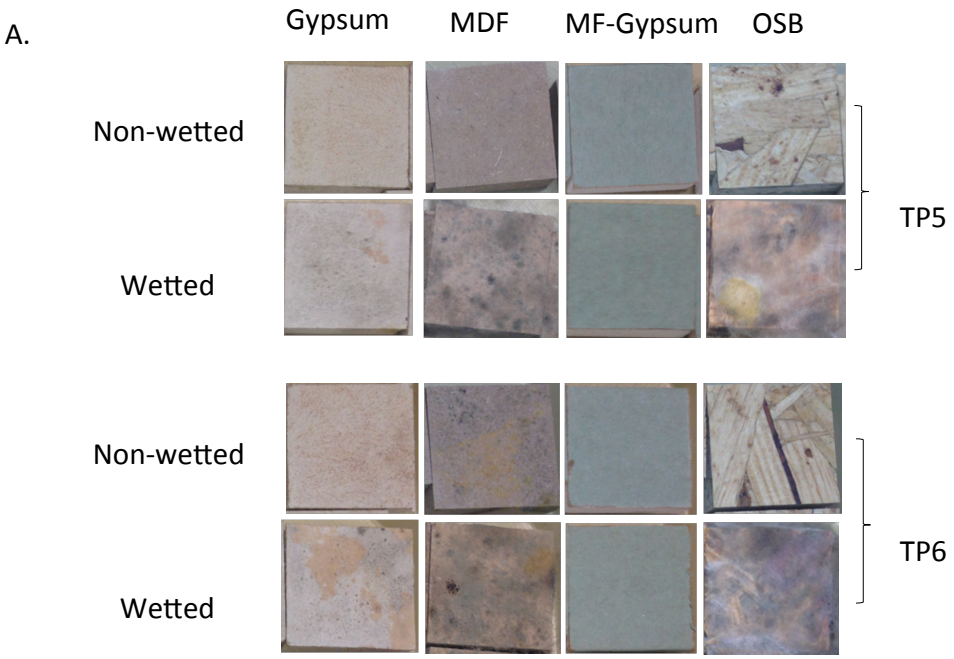

973

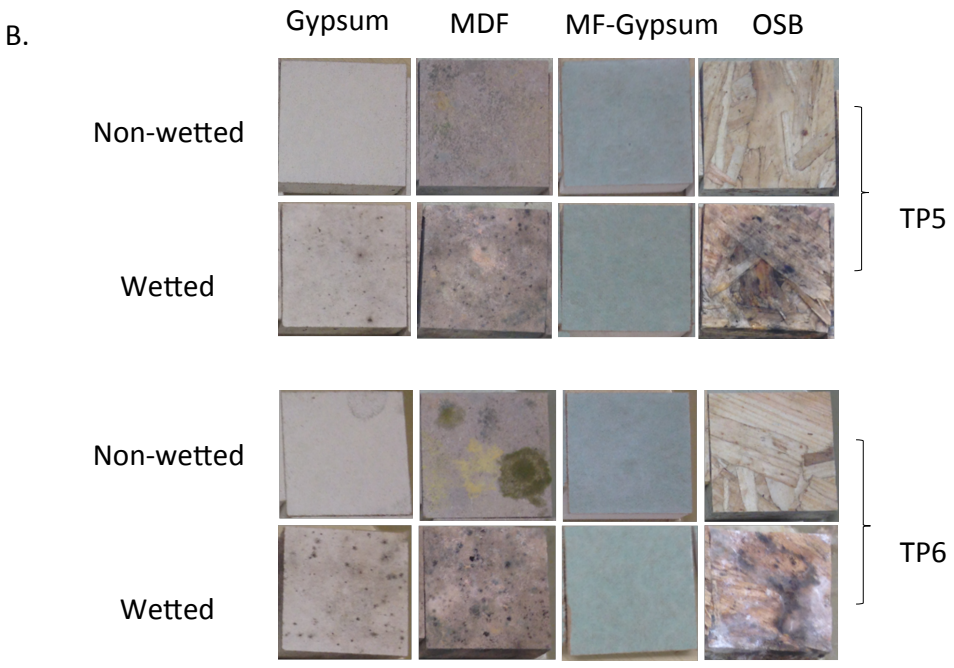

974

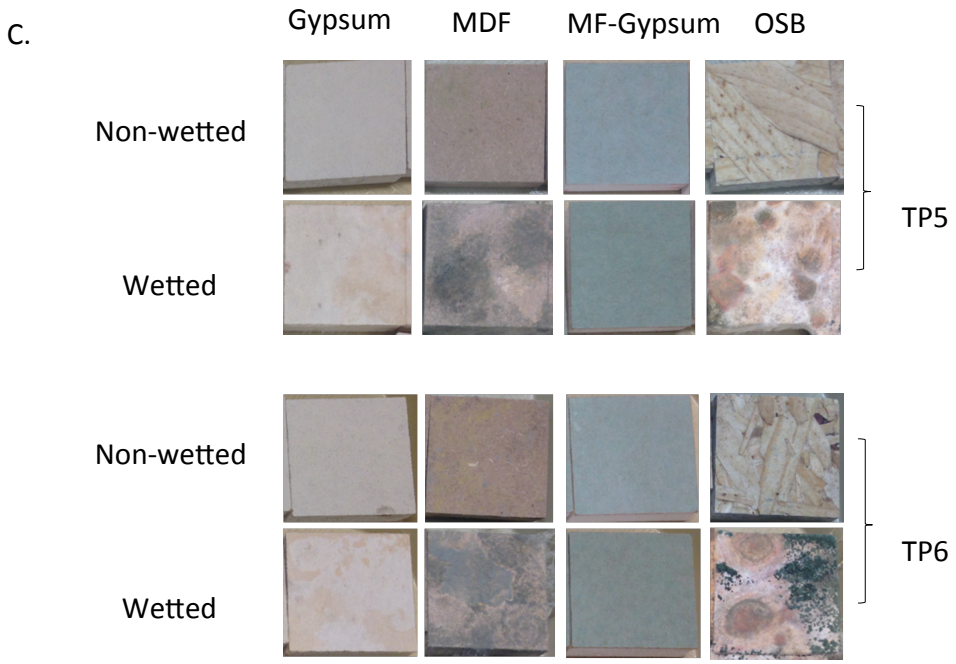

Figure S14: Photographs of wood coupons from different materials and wetting conditions at TP5 and TP6. Bacterial and Fungal growth on coupons surface photographs for (A) location 1 (B) location 2 and (C) control location.

	Bacteria (16S)		Fungi (ITS)		Metabolomics	
	R^2	*p*	R^2	*p*	R^2	*p*
Wetted	0.374	*< 0.0001*	0.450	*< 0.0001*	0.204	*< 0.0001*
Timepoint	0.130	*< 0.0001*	0.094	*< 0.0001*	0.178	*< 0.0001*
Control	0.074	*< 0.0001*	0.107	*< 0.0001*	0.001	*0.983*
Location 1	0.045	*0.0006*	0.076	*0.0006*	0.009	*0.502*
Location 2	0.214	*< 0.0001*	0.303	*< 0.0001*	0.007	*0.603*
Gypsum	0.085	*< 0.0001*	0.022	*0.0271*	0.141	*<0.0001*
MDF	0.108	*< 0.0001*	0.009	*0.2399*	0.238	*<0.0001*
MF Gypsum	0.027	*0.0095*	0.008	*0.2720*	0.209	*<0.0001*
OSB	0.041	*0.0015*	0.002	*0.762*	0.503	*<0.0001*
Bacillus	0.259	*< 0.0001*	NA	NA	NA	NA
Pseudomonas	0.088	*< 0.0001*	NA	NA	NA	NA
Erwinia	0.098	*< 0.0001*	NA	NA	NA	NA
Chloroplast	0.196	*< 0.0001*	NA	NA	NA	NA
Penicillium	NA	NA	0.106	*<0.0001*	NA	NA
Eurotium	NA	NA	0.185	*<0.0001*	NA	NA

Table S1: ANOSIM results calculate the factors significantly correlated with differences in the microbial communities across our three datasets, Bacteria, fungi, Metabolomics

	REG			RE			RE.DUP			DUP		
	mantel	significance	n	mantel	significance	n	mantel	significance	n	mantel	significance	n
REG	<NA>			0.67	1E-05	74	0.71	1E-05	79	0.81	1E-05	44
RE	0.67	1E-05	74	<NA>			0.85	1E-05	77	0.75	1E-05	40
RE.DUP	0.71	1E-05	79	0.85	1E-05	77	<NA>			0.79	1E-05	39
DUP	0.81	1E-05	44	0.75	1E-05	40	0.79	1E-05	39	<NA>		

Table S2: Mantel test results calculate the correlation among fungi samples across different sampling strategies.

	REG			RE			RE.DUP			DUP		
	mantel	significance	n	mantel	significance	n	mantel	significance	n	mantel	significance	n
REG	<NA>			0.62	1E-05	75	0.56	1E-05	75	0.60	1E-05	35
RE	0.62	1E-05	75	<NA>			0.72	1E-05	80	0.53	1E-05	36
RE.DUP	0.56	1E-05	75	0.72	1E-05	80	<NA>			0.50	1E-05	35
DUP	0.63	1E-05	56	0.53	1E-05	36	0.50	1E-05	35	<NA>		

Table S3: Mantel test results calculate the correlation among bacteria samples across different sampling strategies.